Optical chiral metamaterials: a review of the fundamentals, fabrication methods and applications

2016 Nanotechnology 27 412001

(http://iopscience.iop.org/0957-4484/27/41/412001)

IOP Publishing Nanotechnology
Nanotechnology 27 (2016) 412001 (20pp) doi:10.1088/0957-4484/27/41/412001

Topical Review

Optical chiral metamaterials: a review of the fundamentals, fabrication methods and applications

Zuojia Wang[1], Feng Cheng[2], Thomas Winsor[1] and Yongmin Liu[1,2]

[1] Department of Mechanical and Industrial Engineering, Northeastern University, Boston, MA 02115, USA
[2] Department of Electrical and Computer Engineering, Northeastern University, Boston, MA 02115, USA

E-mail: y.liu@neu.edu

Received 11 March 2016, revised 16 April 2016
Accepted for publication 5 May 2016
Published 8 September 2016

Abstract

Optical chiral metamaterials have recently attracted considerable attention because they offer new and exciting opportunities for fundamental research and practical applications. Through pragmatic designs, the chiroptical response of chiral metamaterials can be several orders of magnitude higher than that of natural chiral materials. Meanwhile, the local chiral fields can be enhanced by plasmonic resonances to drive a wide range of physical and chemical processes in both linear and nonlinear regimes. In this review, we will discuss the fundamental principles of chiral metamaterials, various optical chiral metamaterials realized by different nanofabrication approaches, and the applications and future prospects of this emerging field.

Keywords: metamaterial, chiral, nanoscale, plasmonic, nanofabrication

(Some figures may appear in colour only in the online journal)

1. Introduction

Chirality refers to the geometric property of a structure lacking any mirror symmetry plane. It exists in many forms in nature, ranging from molecules, to proteins, and to crystals. In contrast, a structure is achiral if it is indistinguishable or superimposable on its mirror image. Chiral geometries can produce intriguing optical effects. For example, optical activity or optical rotation is the rotation of polarization of linearly polarized light as it travels through a chiral material, while circular dichroism is the differential absorption of left-handed polarized (LCP) and right-handed polarized (RCP) light. Optical activity was first discovered by Arago as sunlight passing through a quartz crystal placed between two crossed polarizers [1]. The optical rotation in quartz originates from the low symmetry of its crystalline structure and highly depends on the wavelength of light. Shortly after Arago's discovery, optical activity of molecules was observed in turpentine (by Biot), and subsequently in solutions of camphor and sugar [1]. Chirality also widely exists in biological species. For example, gyroid nanostructures produce the vivid colors of butterfly wings [2], and chiral microstructure patterns make *Chrysina gloriosa* (jeweled beetles) appear more brilliant under LCP illumination than the case under RCP illumination [3]. Chirality is of great importance in the study of chemistry and biology because molecules with different spatial configurations can lead to distinctly different physiological responses. However, the optical activity of a natural material is generally very weak, and therefore the chiral effect is detectable only when the optical path length is much larger than the wavelength of light.

Metamaterials are artificial composite materials with exotic properties, which have attracted the intensive interest of physicists, material scientists, chemists and engineers over the past few decades. Metamaterials comprise of periodically or randomly distributed artificial structures with size and spacing much smaller than the wavelength of interest [4–7]. Using different metamaterial designs, researchers have been

able to engineer material properties with unprecedented degrees of freedom and demonstrate extremely low-frequency plasmons [8], artificial magnetism [9] and negative refractive indices [10]. One early research focus in metamaterials is to realize negative refractive indices, which promise numerous applications such as super-resolution imaging [11–13], invisibility cloaking [14–18] and illusion optics [19]. Negative permittivity and permeability can be simultaneously achieved in the same frequency band by properly combining electric and magnetic resonators, which gives rise to negative refractive indices. This concept was initially verified at microwave frequencies and then extended deeply into the visible regime [20–24].

As a subset of metamaterials, chiral metamaterials exhibit a number of intriguing properties. For example, if the chirality is sufficiently strong, negative refractive indices can be realized even though neither ε nor μ is negative. Such a chiral route towards negative refractive indices was theoretically proposed by Tretyakov *et al* [25], and later independently discussed by Pendry [26] and Monzon *et al* [27]. This concept was then experimentally demonstrated in the microwave [28–30], terahertz [31] and optical regimes [32, 33]. In addition, chiral metamaterials have attracted much interest because of their extremely strong optical activity [29, 31, 34–37], which promises the ability to create compact broadband circular polarizers [38] and asymmetric transmission [39–42]. Moreover, superchiral electromagnetic fields in chiral plasmonic nanostructures are expected to substantially enhance the interaction between light and chiral molecules by several orders of magnitude [43], which may open a new avenue for chiroptical detection with unprecedented sensitivity.

The rest of the review is organized as follows. We will first discuss in section 2 the symmetry group of chiral metamaterials and its effect on the form of the scattering matrix, followed by the review of optical chiral metamaterials categorized by different nanofabrication approaches in section 3. In section 4, we will survey two aspects of chiroptical effects: extrinsic chirality and the superchiral field. Section 5 will discuss the potential applications of chiral metamaterials, including nonlinear optics, enhanced light–matter interactions and active chiral metamaterials. Finally we will provide a conclusion and a brief perspective on the future development of chiral metamaterials.

2. Chirality parameters and symmetry considerations

As we have discussed, a material is defined as chiral if it lacks any plane of mirror symmetry. In electromagnetics, a chiral medium is a subset of bianisotropic media in which the electrical and magnetic fields are coupled together. For a general chiral medium, the optical response is usually described by the constitutive relations:

$$\overline{D} = \varepsilon_0 \overline{\overline{\varepsilon}} \overline{E} + \frac{\mathrm{i}}{c_0} \overline{\overline{\chi}} \overline{H}, \tag{1}$$

$$\overline{B} = -\frac{\mathrm{i}}{c_0} \overline{\overline{\chi}} \overline{E} + \mu_0 \overline{\overline{\mu}} \overline{H}, \tag{2}$$

where $\overline{\overline{\varepsilon}}$, $\overline{\overline{\mu}}$ and $\overline{\overline{\chi}}$ are the permittivity, permeability and chirality tensors, respectively. ε_0 and μ_0 are the permittivity and permeability of vacuum. $\overline{E}$ is the electric field, $\overline{H}$ is the magnetic field, $\overline{D}$ is the electric displacement and $\overline{B}$ is the magnetic induction. For isotropic chiral materials, the constitutive parameters could be simplified to scalars (ε, μ and χ). The refractive indices for the right- (+) and left-handed (−) circular polarizations are different, and are given by

$$n_{\pm} = \sqrt{\varepsilon\mu} \pm \chi. \tag{3}$$

Equation (3) shows that waves of opposite handedness will obtain different accumulations of phase as they travel through a chiral material. However, the two circular polarizations have the identical impedance of $Z = Z_0\sqrt{\mu/\varepsilon}$, where Z_0 is the impedance of vacuum.

A linearly polarized wave can be described as the superposition of an LCP and an RCP wave with identical amplitude. Starting from equation (3), one can readily prove that the refractive index difference between the two circularly polarized waves leads to the rotation of the linear polarization by an angle $\theta = (n_+ - n_-)\pi d/\lambda_0$, where d is the thickness of the chiral medium and λ_0 is the wavelength of light in vacuum. This is the physical implication and mechanism of optical rotation. Alternatively, the rotation angle can be written as $\theta = [\arg(T_+) - \arg(T_-)]/2$, where T_+ and T_- are the transmission coefficients for the two spin states. For an absorbing chiral medium, the imaginary parts of the refractive index for RCP and LCP light are different, indicating that RCP and LCP light have different attenuation and therefore circular dichroism (CD) occurs. From equation (3) one can also see that if the chirality χ is strong enough, a negative refractive index may exist for one circularly polarized light even when both ε and μ are positive. This is the chiral route to negative refraction as originally proposed by Tretyakov *et al* [25], Pendry [26], and Monzon and Forester [27], and experimentally demonstrated by several groups [28, 31, 32].

The properties of metamaterials are frequently described in terms of effective material parameters, which can be obtained from scattering parameters by the retrieval method [44–46]. However, such an approach requires the tensor format of the complex constitutive parameters to be determined in advance. This feature dramatically increases the complexity in analyzing sophisticated optical effects such as anisotropy, nonlocality and spatial dispersion [47, 48]. As a result, a more suitable means for describing the properties of metamaterials is the optical response itself. For planar metamaterials, the optical responses can be easily described by Jones matrices, which relate the complex amplitudes of the incident and the scattered fields [49, 50].

$$\begin{pmatrix} E_{\mathrm{r}}^{x} \\ E_{\mathrm{r}}^{y} \end{pmatrix} = \begin{pmatrix} \mathrm{r}_{xx} & \mathrm{r}_{xy} \\ \mathrm{r}_{yx} & \mathrm{r}_{yy} \end{pmatrix} \begin{pmatrix} E_{\mathrm{i}}^{x} \\ E_{\mathrm{i}}^{y} \end{pmatrix} = \mathbf{R} \begin{pmatrix} E_{\mathrm{i}}^{x} \\ E_{\mathrm{i}}^{y} \end{pmatrix}, \tag{4}$$

$$\begin{pmatrix} E_{\mathrm{t}}^{x} \\ E_{\mathrm{t}}^{y} \end{pmatrix} = \begin{pmatrix} \mathrm{t}_{xx} & \mathrm{t}_{xy} \\ \mathrm{t}_{yx} & \mathrm{t}_{yy} \end{pmatrix} \begin{pmatrix} E_{\mathrm{i}}^{x} \\ E_{\mathrm{i}}^{y} \end{pmatrix} = \mathbf{T} \begin{pmatrix} E_{\mathrm{i}}^{x} \\ E_{\mathrm{i}}^{y} \end{pmatrix}. \tag{5}$$

Here **R** and **T** are called reflection and transmission matrices for linear polarization. E_{i}^{x}, E_{r}^{x} and E_{t}^{x} are the incident, reflected and transmitted electric fields polarized along the x direction, respectively. The similar notations with a superscript of y represent the fields polarized along the y direction. By changing the Cartesian base to a circular base, the Jones matrices for the two states of circular polarization are obtained [50]

$$\mathrm{R}_{\mathrm{circ}} = \begin{pmatrix} \mathrm{r}_{++} & \mathrm{r}_{+-} \\ \mathrm{r}_{-+} & \mathrm{r}_{--} \end{pmatrix} = \Lambda^{-1}\mathrm{R}\Lambda = \frac{1}{2} \times \begin{pmatrix} \mathrm{r}_{xx} + \mathrm{r}_{yy} + \mathrm{i}(\mathrm{r}_{xy} - \mathrm{r}_{yx}) & \mathrm{r}_{xx} - \mathrm{r}_{yy} - \mathrm{i}(\mathrm{r}_{xy} + \mathrm{r}_{yx}) \\ \mathrm{r}_{xx} - \mathrm{r}_{yy} + \mathrm{i}(\mathrm{r}_{xy} + \mathrm{r}_{yx}) & \mathrm{r}_{xx} + \mathrm{r}_{yy} - \mathrm{i}(\mathrm{r}_{xy} - \mathrm{r}_{yx}) \end{pmatrix}, \tag{6}$$

$$\mathrm{T}_{\mathrm{circ}} = \begin{pmatrix} t_{++} & t_{+-} \\ t_{-+} & t_{--} \end{pmatrix} = \Lambda^{-1}\mathrm{T}\Lambda = \frac{1}{2} \times \begin{pmatrix} t_{xx} + t_{yy} + \mathrm{i}(t_{xy} - t_{yx}) & t_{xx} - t_{yy} - \mathrm{i}(t_{xy} + t_{yx}) \\ t_{xx} - t_{yy} + \mathrm{i}(t_{xy} + t_{yx}) & t_{xx} + t_{yy} - \mathrm{i}(t_{xy} - t_{yx}) \end{pmatrix} \tag{7}$$

where $\Lambda = \frac{1}{\sqrt{2}} \begin{pmatrix} 1 & 1 \\ \mathrm{i} & -\mathrm{i} \end{pmatrix}$ is the change of basis matrix, and the subscript $+/-$ denotes clockwise/counterclockwise circularly polarized waves as viewed along the $+z$ direction, respectively.

Symmetry consideration is an efficient method for predicting how the symmetry of a structure affects the characteristics of the Jones matrices and ultimately the optical properties of the structure. Either rotation or reversion of a structure is accomplished mathematically by applying particular matrix operations. If a metamaterial exhibits a certain symmetry group, the Jones matrices after transformation must be identical to the original ones. We will briefly discuss in the following how mirror and rotational symmetries affect the reflection and transmission matrices of a chiral slab.

The mirror symmetry with respect to the incident plane (defined as the xz-plane) results in the absence of the off-diagonal elements in the Jones matrices of linear polarizations ($r_{xy} = r_{yx} = t_{xy} = t_{yx} = 0$), and thus the Jones matrices for circular polarizations become symmetric ($r_{++} = r_{--}$, $r_{+-} = r_{-+}$, $t_{++} = t_{--}$, $t_{+-} = t_{-+}$) [50]. Since the optical activity is usually characterized by $\theta = [\arg(t_{++}) - \arg(t_{--})]/2$, there is no polarization rotation due to chirality. The off-diagonal elements are also identical so that two circularly polarized waves have the same efficiency of polarization conversion. Therefore, neither optical activity nor circular dichroism can exist in mirror-symmetric structures. This result explains, from the point view of Jones matrix, why chirality only exists in structures that lack mirror symmetries.

In the cases of three-fold (C_3) or four-fold (C_4) rotational symmetries, the symmetry consideration leads to $r_{xx} = r_{yy}$ and $r_{xy} = -r_{yx}$ [50]. For circular polarizations, we therefore obtain $r_{+-} = r_{-+} = 0$. The same reasoning holds true for the transmission matrix so that $t_{+-} = t_{-+} = 0$. In the special case of normal incidence, the De Hoop reciprocity states that the reflection matrix obeys the general identity $\mathbf{R} = \mathbf{R}^{\mathrm{T}}$, where the superscript T represents the transpose operation [51–53]. If we combine these restrictions together, the linear polarization conversions are proved to be zero ($r_{xy} = r_{yx} = 0$). Consequently, the Jones matrices can be written as

$$\mathbf{R}_{\mathrm{circ}} = \begin{pmatrix} \mathrm{r}_{xx} & 0 \\ 0 & \mathrm{r}_{xx} \end{pmatrix} = \mathrm{r}_{xx}\mathbf{I}, \qquad \mathbf{T}_{\mathrm{circ}} = \begin{pmatrix} t_{xx} + \mathrm{i}t_{xy} & 0 \\ 0 & t_{xx} - \mathrm{i}t_{xy} \end{pmatrix}, \tag{8}$$

where **I** is the identity matrix. Therefore, the reflection coefficient is the same for all polarizations, which can also be predicted by the effective medium method. For a structure with C_3 or C_4 symmetry, the expression of the chirality parameter can be simplified to a scalar χ, which leads to the absence of polarization conversions [46, 54, 55]. Calculation in the transmission problem of a chiral slab also reveals that the reflection is identical for both LCP and RCP illuminations in an isotropic chiral material [36]. The underlying reason is that the impedance of such a chiral medium is only determined by the ratio between its permittivity and permeability, and is independent of the chirality parameter. Furthermore, when losses are absent, analyses in reciprocity and energy conservation dictate that the transmission coefficients of the two spin states are also identical [53].

If the chiral metamaterials become anisotropic, such as the two-fold (C_2) rotational symmetry, the polarization conversion between the two spin states in reflection would appear. It is important to note that two-dimensional (2D) planar structures cannot possess structural chirality in a three-dimensional (3D) space. This is because of the equality of the off-diagonal elements in Jones matrices that originated from the in-plane mirror symmetry, which results in $t_{++} = t_{--}$. However, the dichroism in the total transmission of two spin states is still available in well-designed structures, which show unequal efficiencies in polarization conversions ($t_{+-} \neq t_{-+}$) [56]. Such a phenomenon is also termed as asymmetric transmission in reciprocal materials [42, 57]. In addition, metamaterial structures without any rotational symmetries can also exhibit strong chiral responses. For example, twisted-arc structures have been proposed to achieve giant circular dichroism in both microwave [58, 59] and optical frequencies [60, 61]. In these cases, the forms of the Jones matrices can hardly be specified from symmetry considerations and it would be more convenient to analyze the chiroptical responses by the induced current distribution.

Metasurfaces provide a distinct way to manipulate the flow of circularly polarized light [62]. Different from the traditional metamaterials, metasurfaces control the optical responses of circularly polarized light by spatially modulating the phase responses of achiral elements rather than designing chiral metamolecules. A variety of exotic optical phenomena based on this technology have been realized, such as dispersionless abnormal reflection and refraction [63], optical vortex generation [64], optical activity [65], all-dielectric

focusing [66], achromatic generation of optical angular momentum [67] and high-efficiency holograms [68].

3. Fabrication of optical chiral metamaterials

Optical chiral metamaterials, which consist of building blocks with feature sizes on the nanoscale level, can generally be fabricated by the top-down and bottom-up approaches. The top-down approach uses various techniques, such as ion beam lithography, electron beam lithography and direct laser writing, to cut, mill and shape materials into the desired shape and order. The bottom-up approach, in contrast, usually seeks to arrange small components into more complex assemblies. Both of these two fabrication approaches are widely employed to fabricate optical chiral metamaterials as discussed in the following.

3.1. Optical chiral metamaterials fabricated by top-down methods

Chirality is inherently a 3D structural property. One classical example of chiral metamatrials is a 3D helix structure (figure 1). In [38], a uniaxial photonic metamaterial composed of 3D gold helices (figure 1(a)) was investigated as a broadband circular polarizer in the mid-infrared regime. These nanostructures are fabricated by direct laser writing of helical pores followed by electrochemical deposition of gold. To fabricate an array of helical pores, a positive-tone photoresist is selected and spun onto a glass substrate. Only those regions that are sufficiently exposed by light are removed. Deposition of gold is then controlled by the applied current density and the growth time. Plasma etching is finally used to remove the polymer and realize a square array of 3D gold helices on a glass substrate. The measured transmission spectra in the wavelength region from 3.5 to 7.6 μm reveal the anticipated functionality of blocking one direction of circularly polarized light, while transmitting the other circular polarization (figure 1(a)). N-helical [52] and tapered chiral metamaterials [69] have also been designed to reduce the polarization conversion and broaden the operation bandwidth. However, this approach turns out to be impractical for bichiral structures, which consist of both left-handed and right-handed spirals arranged along three orthogonal spatial axes [70]. This is because certain parts of the horizontal helical cavities are cut off from the electrolyte before they can be completely filled, leaving behind gaps in the final structures. Radke *et al* have fabricated bichiral plasmonic crystals by combining direct laser writing with electroless silver plating (figure 1(b)) [71]. First, two-photon femtosecond direct laser writing in a negative-tone photoresist fabricates a 3D bichiral crystal. Next, the dielectric template is coated with a conformal silver film via electroless plating. Electroless plating does not require any external current source and possesses the advantage of coating all exposed surfaces. This feature is very challenging to achieve with standard deposition methods, such as vacuum evaporation and sputter coating, because of the self-shadowing of the complex 3D structures.

Glancing-angle deposition is another approach for fabricating 3D chiral plasmonic nanostructures [72–75]. Its working principle is based on the geometric shadow effect that materials do not deposit in the shadow created by existing structures. Plasmonic nanohelices have been fabricated via the technique of low-temperature shadow deposition [74, 76]. Through precise control over the nanoseed pattern, substrate and temperature, nanohelices of opposite handedness have been successfully fabricated. The measured circular dichroism spectra of the nanohelices in sodium citrate solution show a peak for LCP light and a dip for RCP light around 600 nm (figure 1(c)). Chiral gold nanoshells have also been made by vacuum evaporation on achiral nanopillars with tilted deposition angles [72]. Large-area 3D gold spirals have also been manufactured by colloidal hole-mask lithography in combination with tilted-angle rotation evaporation (figure 1(d)) [77]. Control over both the rotating speed and direction of the samples can flexibly switch the handedness and working frequency of chiral enantiomers. Circular dichroism signals up to 13% have been measured in the 100–400 THz frequency range. This method offers a simple low-cost manufacturing method for cm^2-sized chiral plasmonic metamaterials. Another method for fabricating 3D chiral materials is on-edge lithography [78]. In this approach, a template with a corrugated profile is first generated. Then, a thin chromium layer is deposited by physical vapor deposition, followed by spin coating of a layer of electron beam resist. The resist is subsequently exposed and the resulting mask is evaporated with a layer of gold. The 3D L-shape is finally obtained after lift-off (figure 1(e)). This fabrication approach offers an accurate method for generating 3D chiral nanostructures within a single lithography step.

Focused ion beam induced deposition (FIBID) has recently been employed for realizing broadband chiral metamaterials in the near-infrared region [79]. Platinum nanospirals are formed by FIBID and scanning electron microscopy (SEM) in a dual configuration system. Precursor metal–organic compounds are decomposed by an ion beam and absorbed onto the substrate. The handedness of nanospirals is controlled via sweeping the ion beam in a clockwise or counterclockwise direction. Surface charge effects on different substrates can influence the growth and evolution of nanostructures and induce a dimensional gradient of the wire diameter of the spiral structure. Multiple-helical structures have been created using tomographic rotatory growth, which combines the basic principles of tomography with the FIBID technique (figure 1(f)) [80]. Rotational symmetry is ensured by a packed multi-helix arrangement in a single cell, which eliminates cross-polarization conversion from anisotropy. These triple-helical nanowires show up to 37% of circular dichroism in a broad range from 500–1000 nm.

Focused electron beam induced deposition (FEBID) is also a suitable technique for the realization of three-dimensional nanostructures for optical applications [81–83]. Nanoscaling of chiral structures has been achieved by comparing the FIBID and FEBID approaches [84]. Some physical factors affecting the fabrication processes, including

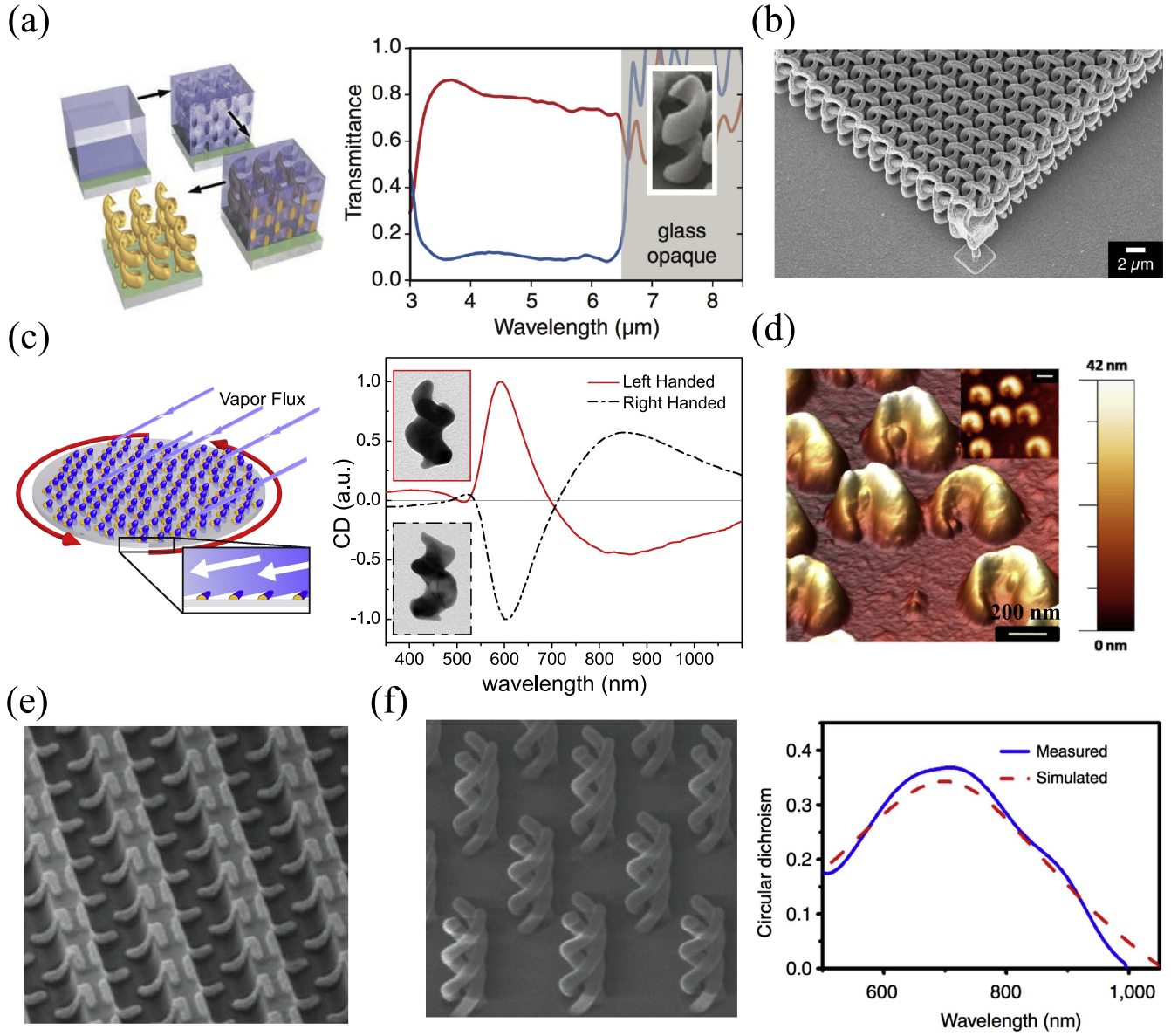

Figure 1. 3D chiral metamaterials fabricated by top-down methods. (a) Fabrication process of 3D helices by direct laser writing and electrochemical deposition of gold (left panel) and the transmission spectra in the mid-infrared region for structures with opposite handedness (right panel). (b) SEM image of a bichiral crystal with right-handed corners and left-handed helices after electroless silver plating. (c) Glancing-angle deposition of nanohelices and the CD spectra. Inset: transmission electron microscopy (TEM) images of grown structures with left (top) and right (bottom) chirality. (d) Atomic force microscopy (AFM) image of 3D spirals fabricated by colloidal hole-mask lithography. (e) SEM image of 3D L-shape nanostructures fabricated by on-edge lithography. (f) SEM image and CD spectra of triple-helical nanowires fabricated by tomography rotatory growth, on the basis of FIBID. (a) is adapted from [38], (b) is adapted from [71], (c) is adapted from [74], (d) is adapted from [77], (e) is adapted from [78] and (f) is adapted from [80] with permissions.

resolution limits, growth control and 3D proximity effects, have been carefully analyzed.

Stacked-planar structures are an alternative approach to accomplishing strong chiroptical responses. In general, such structures can be fabricated by standard electro-beam lithography along with alignment in a layer-by-layer manner. Figure 2(a) shows a chiral structure of twisted split rings [85]. The transmittance spectrum can be tuned by adjusting the twisted angle. Specifically, when the angle is 90°, the electric fields in the gaps of the two split rings are perpendicular to each other and thereby no electric dipole–dipole interaction occurs. In addition, as the higher-order multipolar interaction is negligible in a first approximation, the electric coupling can be ignored. Therefore, the resonances are determined by magnetic dipole–dipole coupling. For the 90° twisted dimer, the magnetic dipoles in the two split rings at the two resonances (ω_{90}^{-} and ω_{90}^{+}) are aligned parallel and antiparallel, respectively, and thus produce chiroptical responses. This strategy is similar to the concept of stereoisomers in chemistry in that isomers have identical chemical formula but different spatial arrangements of atoms in a molecule. It is known that the electronic properties of a molecule are generally influenced by its composite as well as its configuration. These properties determine how the electronic wave functions mix

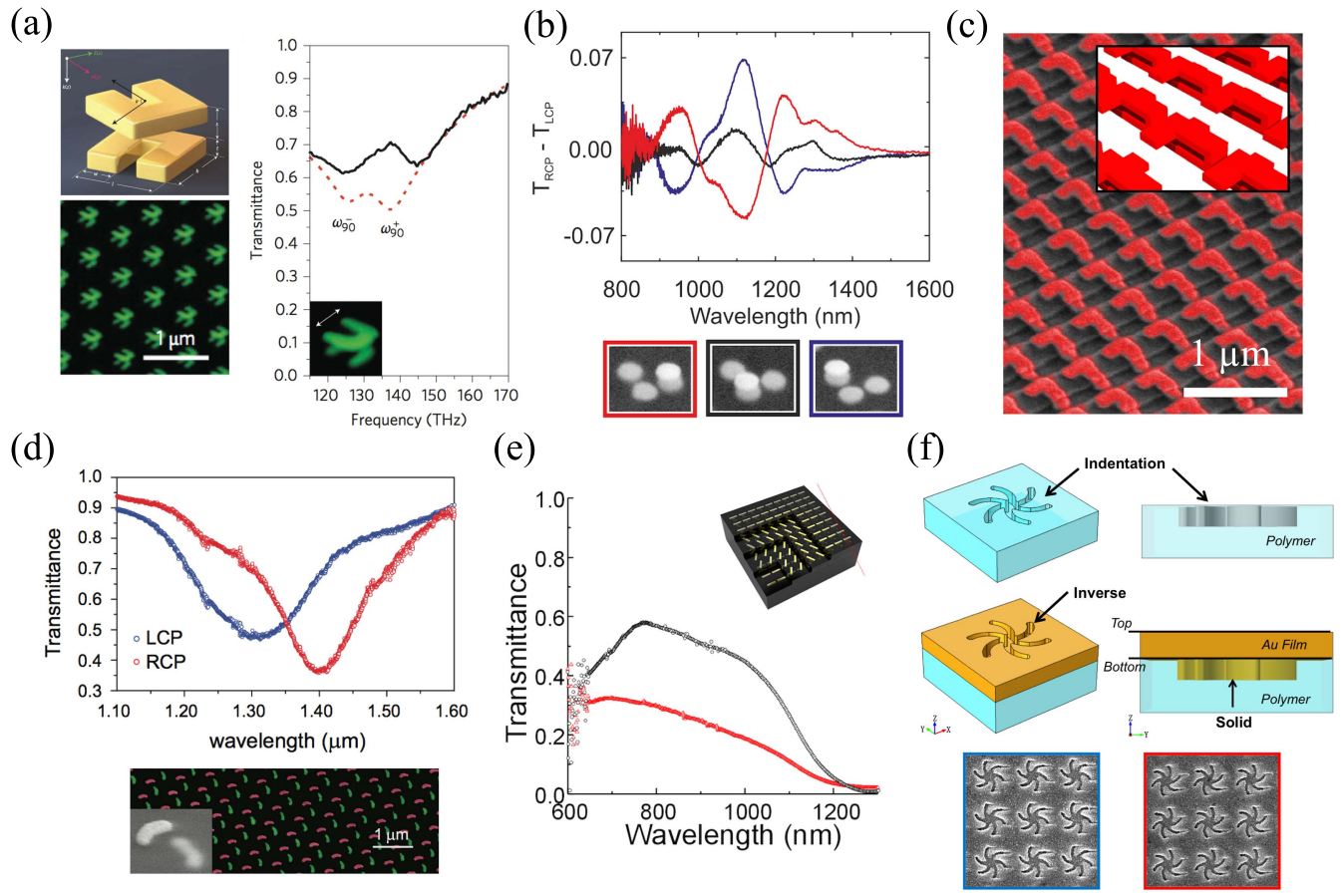

Figure 2. Stacked-planar chiral metamaterials. (a) Schematic, field-emission electron microscopy and transmission spectra of a twisted gold split-ring dimer metamaterial. (b) CD spectra and SEM images of three chiral oligomers. (c) L-shape chiral nanostructure. (d) Twisted-arc chiral metamaterials and the corresponding transmission spectra. (e) Multilayer twisted metamaterial as a broadband circular polarizer. (f) Schematic and SEM images of chiral metamaterials fabricated by depositing gold film on structured polycarbonate substrates. (a) is adapted from [85], (b) is adapted from [87], (c) is adapted from [90], (d) is adapted from [60], (e) is adapted from [95] and (f) is adapted from [96] with permissions.

and hybridize, as well as the interaction and binding between the atoms in the molecule [86]. Similarly, a cluster composed of several nanoparticles provides the possibility of configuring the hybridization of plasmonic resonances, thus enhancing the overall chiroptical responses in plasmonic oligomers (figure 2(b)) [87–89]. Diverse chiral nanostructures have been proposed based on this methodology, including bilayer L-shapes (figure 2(c)), arcs (figure 2(d)) and so on [32, 60, 90–94].

Broadband circular dichroism can also be achieved by cascading multilayer identical nanorod metasurfaces with a relative rotational twist [95]. As shown in the schematic of figure 2(e), each layer of nanorod is intrinsically achiral. Nevertheless, the chiroptical response emerges when neighboring layers are stacked in a helical-like fashion. The transmission spectra of the four-layer twisted structure demonstrate a broadband circular dichroism in the visible regime. Some constraints can be relaxed in such planar, twisted chiral structures, including the complexity of shape requirements and the lateral alignment between neighboring layers. Moreover, a disposable plasmonic chirality has been recently proposed, where a metafilm is grown on a nanoindented polycarbonate substrate fabricated by high-throughput injected molding [96]. The generated structure consists of a solid nanostructure and an identical shaped void directly above it (figure 2(f)). Babinet's principle implies that the switch of electric and magnetic fields between the solid and inverse structure gives rise to the chiroptical response. The optical properties can be tuned by changing the film thickness. This method offers a cost-effective and flexible way of manipulating the chirality in plasmonic structures.

3.2. Self-assembled chiral nanostructures

While top-down fabrication technologies are capable of precisely making nanostructures with a feature size of or below 100 nm, they are normally non-scalable, time-consuming and expensive. By contrast, self-assembly technology provides an alternative bottom-up approach for realizing structures at the truly nanometer scale yet in a cost-efficient, highly-tunable and fast manner. Over the past few years, self-assembled chiral nanostructures have attracted extensive interest and shown significant progress.

Self-assembly technology takes advantage of the fundamental forces of nature to synthesize building blocks into

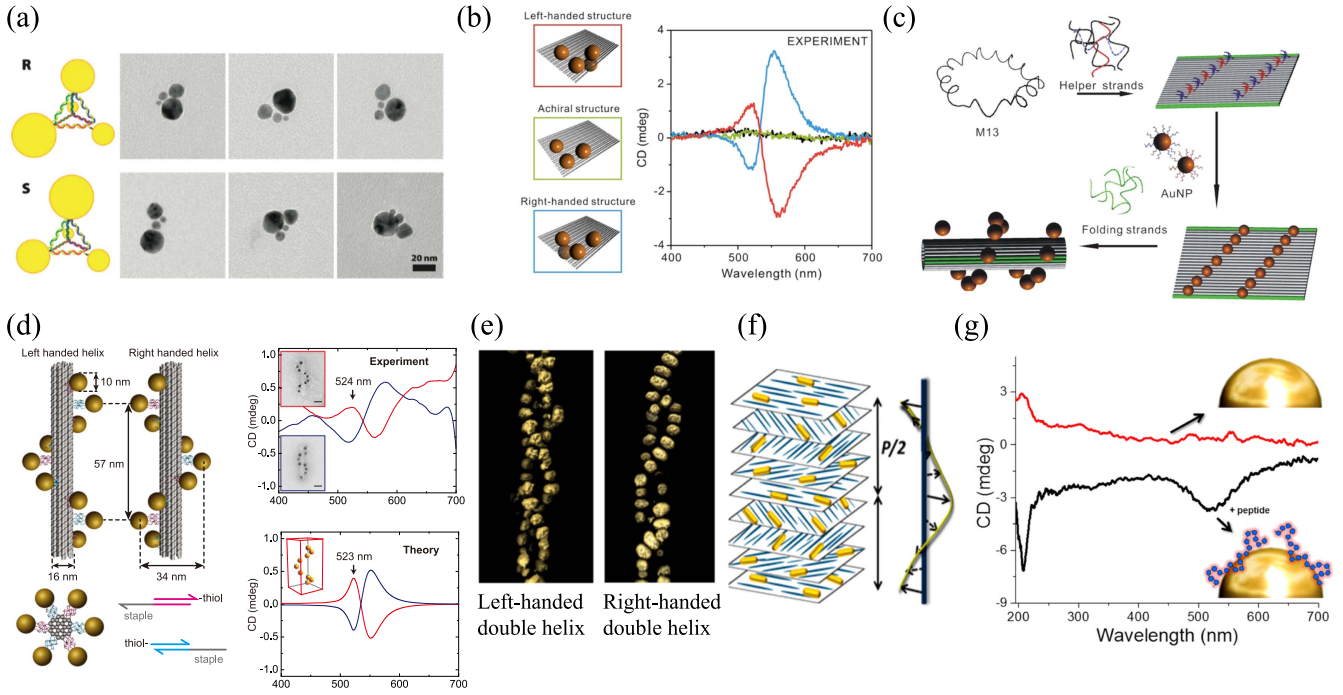

Figure 3. Plasmonic chiral nanostructures based on a self-assembly method. (a) Illustration of chiral pyramids of gold nanocrystals obtained with DNA scaffolds and TEM images. (b) Four gold nanoparticles assembled with bifacial DNA template in left-handed, right-handed and achiral structures and the corresponding CD spectra of these structures. (c) Illustration of synthesizing a 3D gold-particle helix by rolling a planar DNA template into a 3D DNA origami tube. (d) Schematic illustration of DNA-guided self-assembly of plasmonic nanohelices with both left and right handedness and the corresponding CD signals. (e) Double-helix nanoparticle superstructures by peptide-based assembly platforms. 3D surface renderings of the tomographic volumes show the left-handed or right-handed structure of double helices. (f) Schematic of chiral plasmonic nanostructures assembled with gold nanorods and cellulose nanocrystals. (g) Enhanced chiral dichroism after binding gold nanoparticles with peptide molecules that have chiral properties. (a) is adapted from [101], (b) is adapted from [106], (c) is adapted from [112], (d) is adapted from [113], (e) is adapted from [119], (f) is adapted from [120] and (g) is adapted from [134] with permissions.

multi-atom functional systems. Objects at the nanometer scale can be organized into equilibrium structures due to the delicate balance among various forces [97, 98], which include Van der Waals forces, capillary forces, static and/or transient electromagnetic forces, convective forces, friction forces, and so on. Based on such self-assembly methods, various metallic nanoparticles with different chemical compositions, geometries and sizes can be precisely positioned and controlled. As a result, plasmonic structures with tunable and controllable dimensions can be assembled in a programmable manner with nanometer precision.

The DNA base-pair interaction is widely used for the synthesis of plasmonic chiral nanostructures. DNA-based formation of silver nanoparticles with CD properties has been demonstrated in some early work [99, 100]. Metallic nanoparticles can also be assembled into pyramid geometries with DNA to enhance the chiral responses [101, 102]. In [101], Mastroianni *et al* demonstrated chiral pyramidal nanostructures, in which DNA strands function as a scaffold for controlling the position of gold nanoparticles with different diameters. The TEM images of synthesized chiral pyramids are shown in figure 3(a). This work provides a way of creating artificial multi-atom molecules with controllable optical properties. The building blocks in such multi-atom molecules are not limited to gold nanocrystals. It is possible to link other metallic and semiconductor particles via this method. Theoretical modeling for such pyramid structures has been performed [103, 104]. The pyramidal structure consists of two pairs of nanoparticles with different sizes. The intensity, spectral characteristics and handedness of the CD response can be tuned by changing the separation along the symmetry-breaking arm. Simulations predict significant CD tunability when the length of the symmetry-breaking arm is varied [104].

Bifacial DNA origami templates can also be used to fabricate chiral nanostructures with metallic nanoparticles [105–107]. For example, it has been reported that bifacial DNA origami templates can be used to assemble 3D chiral metamaterials with four gold nanoparticles [106]. The experimental schema is shown in figure 3(b). The rectangular DNA origami template is predesigned with three binding sites on the top surface and the fourth site on the bottom surface, right below one of the three top binding sites. Left-handed and right-handed structures can be obtained by setting the fourth binding sites in the left-handed or right-handed geometry. A characteristic bisignate CD spectrum is observed for left-handed and right-handed chiral nanostructures, compared with achiral nanostructures.

The idea of folding DNA strands to create artificial nanostructures [108–110] has stimulated the rapid development of plasmonic chiral metamaterials [111–114]. One experimental study of DNA-based chiral metamaterial is shown in figure 3(c) [112]. The gold nanoparticles coated with special DNA strands are able to bond with

complementary DNA strands on the rectangular template at predesigned positions. Upon the use of folding strands, the rectangular DNA template will roll up and eventually become a 3D DNA origami tube. This DNA 'origami' method enables the synthesis of both left-handed and right-handed metamaterials [113], which exhibit pronounced CD responses as shown in figure 3(d). As expected, the signal of the left-handed chiral plasmonic metamaterials and the signal of the right-handed ones are complementary to each other. The CD spectrum can be controlled by depositing additional silver or silver–gold alloy shells on the gold nanoparticles. Since silver has a plasmonic resonance at a shorter wavelength, a blue shift of the CD resonance can be achieved when changing the metal composition.

Assembling metallic nanoparticles with other chiral templates has also been widely studied, such chiral templates are organogel [115], cysteine [116], peptide [117–119], cellulose nanocrystals [120–123], cholesteric liquid crystals [124–128], chiral mesoporous silica [129, 130], supramolecular fibers [131] and block copolymer templates [132, 133]. For example, one work demonstrated the self-assembly of cysteine (CYS) and gold nanorods [116]. Opposite CD responses were observed for L- and D-CYS assembled gold nanorods, while no chiral responses were observed for DL-CYS. The CD responses can be manipulated from visible to near-infrared wavelengths by changing the aspect ratios of the assembled CYS and gold nanorods. Plasmonic chiral nanostructures can be also synthesized through a peptide-based methodology [119]. As shown in figure 3(e), mixing a gold nanoparticle precursor solution and a HEPES buffer with C_{12}–L-PEP_{au} or C_{12}–D-PEP_{au} will form left-handed or right-handed double-helix structures, respectively, which produce strong CD responses. The CD signal can be controlled by varying the thickness of the silver coating. In another work [120], plasmonic chiral metamaterials with cellulose nanocrystals have been assembled. The cellulose nanocrystals are rod-like nanoparticles that were self-assembled into cholesteric liquid crystalline phases. The nanoparticles were highly crystalline and negatively charged with high concentration in suspensions. Chiral plasmonic films were prepared by incorporating gold nanorods in self-assembled cellulose nanocrystals that have chiral arrangements, as shown in figure 3(f). A blue shift in the CD spectrum was observed as the concentration of nanorods increases. The chiral optical activity can be tuned by changing nanorod dimensions and the helical pitch of the cellulose nanostructure. The helical pitch can be tuned by adding NaCl to the nanorod-cellulose nanocrystal suspensions.

Last but not least, plasmonic chiral nanostructures can be realized by binding chiral molecules with metallic nanoparticles [134–137]. In one study [136], plasmonic enhancement of the CD spectrum was demonstrated through the attachment of l-GS-bimane chromophore to the surfaces of the silver nanoparticles. The two orders of enhancement in magnitude made it possible to observe a very weak induced CD signal of the bimane chromophore [136]. It was also found that chiral dichroism can be induced by binding peptide molecules on gold nanoparticles [134], as shown in figure 3(g). Two types of hybrid structures have been studied. One is E5–AuNPs, in which E5 is a 38 amino acid helical peptide that links with the gold nanoparticles through a thiol linkage. The other is FlgA3–AuNPs, where the FlgA3 peptide is an unstructured random coil peptide that binds gold nanoparticles via noncovalent interactions. The chiral responses of two kinds of hybrid structures have been observed.

4. Chiroptical effects

4.1. Extrinsic chirality

It is worth noting that optical activity can be observed even when the structures are intrinsically achiral in geometry (figure 4). Such extrinsic chirality arises from the mutual orientation of the achiral metamaterials and the incident beam. This mechanism was detected in liquid crystals in the past [138], but only revisited recently in achiral metamaterials [139]. As shown in figure 4(a), using asymmetric split rings, researchers have observed strong circular dichroism and birefringence indistinguishable from those of chiral 3D materials. The underlying mechanism is the simultaneously induced electric and magnetic dipoles that are parallel to each other. The oblique incidence is crucial for observing extrinsic chirality, because it breaks the mirror symmetry for any plane containing the wave vector (propagating direction). Extrinsic chirality can also induce a large circular dichroism in individual single-walled carbon nanotubes, with the degree of polarization reaching 65% [140]. Moreover, electromagnetic chirality can occur in 1D patterned composites whose components are achiral [141]. A schematic diagram is given in figure 4(b). Electromagnetic waves propagate through a 1D metamaterial whose unit cell is obtained by stacking layers of different media of different thickness along the x-axis. In the epsilon-near-zero regime, the nonlocal effect can be comparable or even greater than the local linear part of the dielectric response and results in enhanced chiroptical responses.

Extrinsic chirality in anisotropic plasmonic metasurfaces can be greatly boosted by interaction with evanescent excitations [142]. Figure 4(c) schematically illustrates the process in which the incoming light of opposite handedness impinges onto an array of gold nanoparticles. When illuminated slightly above the critical angle, no transmission is allowed. For incident wavelengths close to the plasmonic resonance of the nanoparticles, the metasurface can efficiently absorb the LCP light while the other spin state is almost totally reflected. The effect of photon spin selectivity originates from the mutual orientation of the achiral metasurface, so-called extrinsic chirality, and highly depends on both the incident angle and the relative orientation of the nanoparticle. Almost perfect selectivity (~90%) of the incident photon spin has been observed at visible frequencies. Since polarization manipulation has intriguing applications in photonics, the enhanced chiroptical effects from evanescent waves may pave a new way for efficient on-chip chiroptical devices.

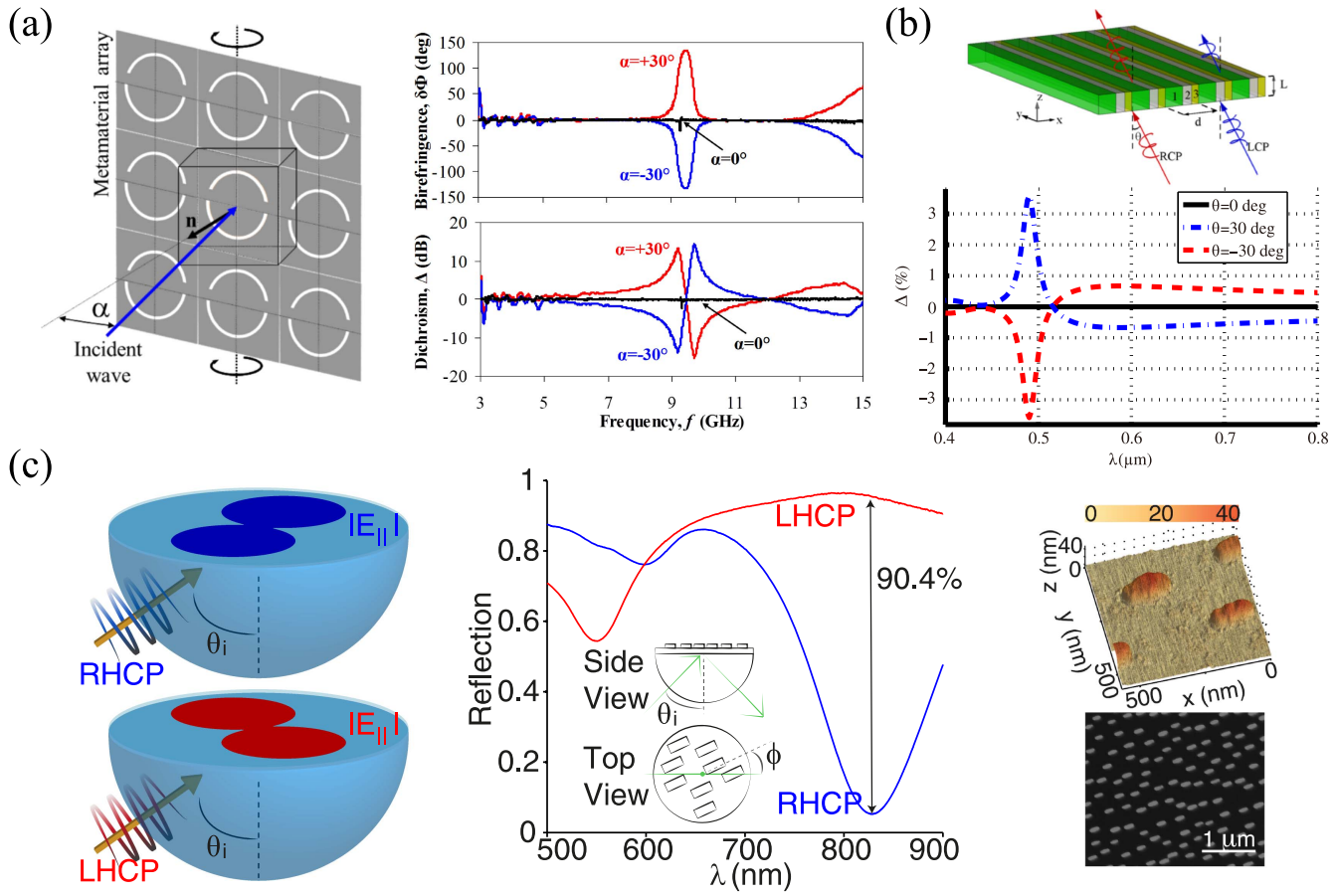

Figure 4. Extrinsic chirality. (a) Planar metamaterials based on an array of asymmetrically split rings manifest optical activity and circular dichroism at oblique incidence of light. (b) One-dimensional multilayer metamaterials show chirality in the epsilon-near-zero regime. The bottom panel depicts the optical activity of such a slab. (c) A randomly arranged anisotropic metasurface exhibits a near-complete photon spin selectivity under evanescent excitations. The left panels show the in-plane electric field amplitudes. The middle panel depicts the reflection spectra. The right panels are the AFM and SEM images of the elongated gold nanoparticles. (a) is adapted from [139], (b) is adapted from [141], and (c) is adapted from [142] with permissions.

4.2. Superchiral fields

Molecules of opposite chirality, called enantiomers, always show identities in almost all physical properties (e.g., density, weight, electronic and vibrational frequencies). Opposite enantiomers become distinguishable only when they interact with other chiral objects, such as circularly polarized light. Therefore chirality-sensitive spectroscopic techniques, including circular dichroism, optical rotatory dispersion and Raman optical activity, are widely used in biomolecular science [1, 143]. However, the inherently weak chiroptical effect of molecules imposes significant challenges in biomolecular detection, especially when the concentration of molecules is low. In recent years, chiral plasmonic metamaterials have aroused a lot of interest because their chiroptical effects can be several orders of magnitude higher than those of common biomolecules [34, 144]. Furthermore, chiral plasmonic metamaterials can efficiently enhance the optical signals from biomolecules [145–148]. This is because of the enhancement of the chiral field in the near-field region, known as the superchiral field, which may provide a method for detecting the handedness of a single molecule.

The optical chirality C, a time-even pseudoscalar, is used to quantify the enhancement of this light–matter interaction [149–151]

$$C(\bar{r}, t) = \frac{1}{2}\left[\varepsilon_0 \overline{E}(\bar{r}, t) \cdot \nabla \times \overline{E}(\bar{r}, t) + \frac{1}{\mu_0}\overline{B}(\bar{r}, t) \cdot \nabla \times \overline{B}(\bar{r}, t)\right], \quad (9)$$

where $\overline{E}$ and $\overline{B}$ are the time-dependent electric and magnetic fields, respectively. Although the quantity of chirality C was introduced in 1964, the physical meaning was disclosed very recently [151]. It has been demonstrated that this quantity is closely related to the rate of excitation of a chiral molecule. If one can increase the chirality C at the location of chiral molecules, the sensitivity for the detection of the handedness can also be enhanced [151, 152]. For time-harmonic fields, chirality C can be written as a simpler version [43]

$$C(\bar{r}) = -\frac{\omega\varepsilon_0}{2}\mathrm{Im}[\overline{E}^*(\bar{r}) \cdot \overline{B}(\bar{r})]. \quad (10)$$

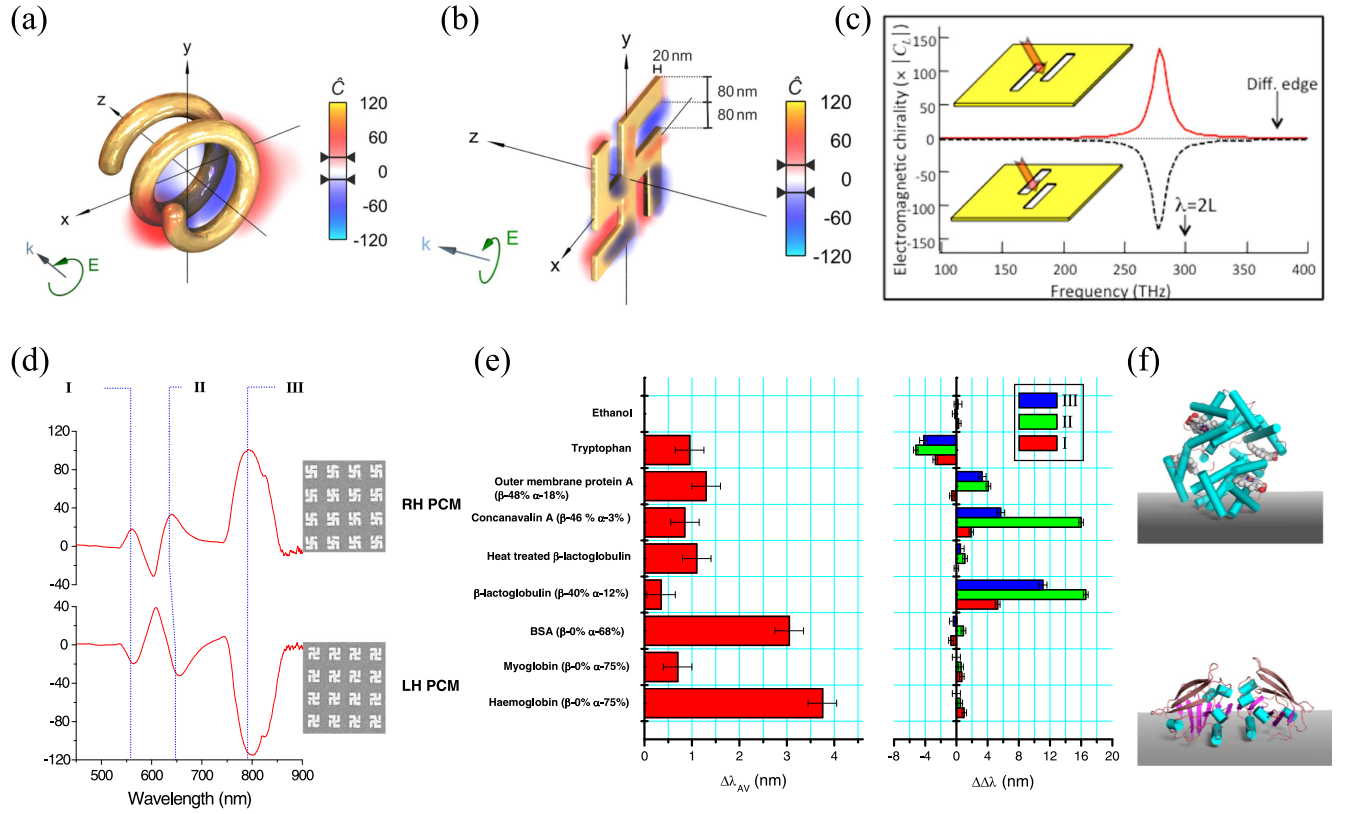

Figure 5. Superchiral field. Optical chirality enhancement for (a) a left-handed helix and (b) a planar gammadion with left-handed circularly polarized light. (c) Local electromagnetic chirality in the center of nanoslit pairs, 1 nm above the transmission interface of the array. Solid and dashed lines represent the two enantiomers. (d)–(f) Superchiral field-based biosensing. (d) CD spectra of left-handed/right-handed planar chiral metamaterials. (e) The averaged resonance shift (left) and difference in resonance shifts (right) between right-handed and left-handed planar chiral metamaterials on adsorption of chiral biomolecular layers. (f) Hemoglobin (top) and β-lactoglobulin (bottom) molecules adopt different geometries upon adsorption due to their secondary structures (α-helix, cyan cylinders; β-sheet, ribbons). (a) and (b) are adapted from [43], (c) is adapted from [153], and (d)–(f) are adapted from [145] with permissions.

Since the maximum optical chirality in free space is obtained for circularly polarized light $C_{\mathrm{CPL}}^{\pm} = \pm\frac{\omega\varepsilon_0}{2c}|\overline{E}|^2$, where ω is the angular frequency and c is the velocity of light in vacuum, the relatively local enhancement of chirality can be calculated by $\hat{C}^{\pm} = C^{\pm}/|C_{\mathrm{CPL}}^{\pm}|$. The positive and negative signs correspond to the right-handed and left-handed circular polarizations defined from the point of view of the source, respectively.

Recent work has shown that plasmonic nanostructures, whose geometry directly influences the distributions of their near fields, can be utilized to generate chiral fields with strong optical chirality. Interestingly, this strong optical chirality exists not only in 2D and 3D chiral structures under circularly polarized illuminations [43], but also in achiral structures illuminated by linearly polarized light [153–155]. For example, figure 5(a) shows the optical chirality of a left-handed helix with left-handed circularly polarized light. The absolute values of optical chirality are much smaller for the nonmatching configurations, in which the same structure is illuminated with the opposite spin state. Planar gammadion also exhibits a similar behavior for circularly polarized light, as illustrated in figure 5(b). However, the gammadion shows both positive and negative optical chirality with similar strength, while for the helix the values corresponding to the nonmatching configuration are much smaller. Moreover, in gammadion structures, regions with enhanced optical chirality are at the same position and have same signs for both spin states. Therefore, a change of incident polarization cannot provide a large change in the optical chirality at a certain position, which makes this design less practical in applications. Interestingly, the chiral near fields can also be formed in achiral structures [153, 154]. For example, optical chirality occurs in the near field of nanoslit pairs illuminated with linear polarized light (figure 5(c)) [153].

An experimental study of superchiral fields for biosensing was reported in [145], which employed gold gammadion arrays working at visible and near-infrared frequencies. As shown in figure 5(d), three resonant modes exist in this planar chiral metamaterial. The spectra of the left-handed and right-handed gammadions are mirror images of each other, as expected. By coupling the incident light into localized surface plasmon resonances of the gold nanostructures, the local chiral field is greatly enhanced and thereby molecules adsorbed on the surface of the chiral metamaterials will strongly influence the resonant wavelength. The property of resonance shifts is caused by the change in the refractive index, which is determined by the chirality of the molecules and that of the fields. According to the first line in figure 5(e),

almost no shift is observed for an achiral adsorption such as ethanol. Specifically, large dissymmetry is observed in the difference in resonance shifts of tryptophan and β-sheet proteins. The measured results also provide indirect information on the geometry of chiral molecules, which can be used to explain the asymmetric difference in the resonance shifts. As shown in figure 5(f), biomacromolecules rich in α-helices are more isotropically distributed at the interface, while the β-sheet proteins result in anisotropic aggregation in lateral directions.

5. Applications

5.1. Nonlinear optics in chiral metamaterials

The application of chirality in biochemical engineering is not limited to the linear regime. In fact, chiroptical effects in second-harmonic generation (SHG) are typically orders of magnitude larger than their linear counterparts [156–158]. In the second-harmonic process, two photons at a fundamental frequency are annihilated into a single photon at twice the frequency [159]. This response can be described by a nonlinear polarization, which can be written in the electric dipole approximation as $P_i^{\mathrm{NL}}(2\omega) = \chi_{ijk}^{(2)} E_j(\omega) E_k(\omega)$, where ω is the angular frequency, $\chi_{ijk}^{(2)}$ is the second order susceptibility tensor, E is the electric field and i, j, and k are the Cartesian indices. By applying the inversion symmetry to this equation, we can find that SHG only exists in noncentrosymmetric materials or matter that lacks inversion symmetry. Thus chiral metamaterials are naturally suitable for SHG because all chiral structures are intrinsically noncentrosymmetric. Based on this concept, researchers have performed SHG measurements to detect the handedness of planar G-shape nanostructures [144, 160, 161], as well as twisted-cross gold nanodimers [162]. It has been demonstrated that the chirality can be distinguished with linearly polarized light regardless of the polarization direction and the polarization state of the second-harmonic light [160].

To better understand the underlying physics of the nonlinear process in chiral nanostructures, the relationship between second-harmonic responses and superchiral fields was investigated in [163]. Traditional Slavic symbols (gammadions) were chosen in the experiments, and the separation distance between neighboring units was gradually decreased from 493 nm to 64 nm. Simulation results indicated that the strong density of optical angular momentum at interfaces can give rise to the enhancement of a localized superchiral field and thus strong second-harmonic signals are observed in experiments. In addition, whereas conservation under space and time reversal causes the linear response in chiral metamaterials to be reciprocal, it has also been indicated that the nonlinear ones are in fact non-reciprocal [163]. CD spectra show that CD does not change its sign upon flipping the sample, which is generalized as reciprocal chiroptical behavior. In the nonlinear regime, however, the SHG-CD does change its sign. These findings provide the means for experimental mapping of the local superchiral fields and design guidance for plasmonic devices with strong chiral light–matter interactions. Based on this fact, the separation distance of neighboring units was optimized to enhance the macroscopic circular dichroism in the second-harmonic field (figure 6(a)). Strong SHG-CD signals have also been observed in twisted-arc structures that lack the four-fold rotational symmetry [61]. An image of the 'GT' logo has been created by a point-by-point calculation of the SHG-CD (figure 6(b)). In addition, anisotropic SHG-CD measurements in four-fold symmetric G-shaped nanostructures have demonstrated that both the value and the sign of the CD response are highly dependent on the incident angles of the fundamental illuminations [161]. The SHG probe can thereby also serve as an extremely sensitive probe of the structural symmetry, and allow us to distinguish between chirality and anisotropic effects.

Chiroptical effects in the second-harmonic field have also been investigated in anisotropic achiral structures [164, 165]. Figure 6(c) shows the measured circular dichroism in the second-harmonic field. Blue circles show the measured SHG-CD for the sample with the curvature of nanowires pointing down. The SHG-CD increases as the incident angle becomes larger. The situation is reversed when the sample is rotated by 180 degrees (red circles). Specifically, the achiral structure of curved nanowires has shown more than 50% visibility by exploiting the extrinsic chirality in the second-harmonic field [165].

5.2. Chiral light–matter interactions

The enhancement of chiral light–matter interaction is one of the research focuses in chiral metamaterials. Superchiral fields, as discussed before, have been suggested to overcome the problem of weak chiroptical signals in nature. Subsequently, significant effort has been given to find various nanostructures that enhance chiroptical signals, such as plasmonic structures [43, 145, 153, 155], dielectric nanoparticles [166] and negative-index metamaterials [167]. The chiral Purcell factor has also been proposed for characterizing the ability of optical resonators to enhance chiroptical signals [168]. In [169], the effect of parity-time symmetric potentials on the radiation of chiral dipole sources has been theoretically investigated. Through appropriate design of parity-time symmetric potentials, chiral quantum emitters can be distinguished by their decay rates.

The interaction between quantum emitter and chiral metamaterials has been experimentally investigated in [170]. In this work, chiral arc metamaterials were adopted as the two enantiomers, as shown in figure 7(a). Achiral quantum dots occupied the entire space around the upper arc and only a slight part of the lower arc. In the linear regime, the circular dichroism of the arc metamaterials reached as high as 50% at the wavelength of resonance (~780 nm), which led to the highest contrast of the transmission images of the chiral metamaterials patterned into the Georgia Tech mascot. The light confinement at the resonant wavelength was largely boosted and thereby implied a chiral-selective enhancement

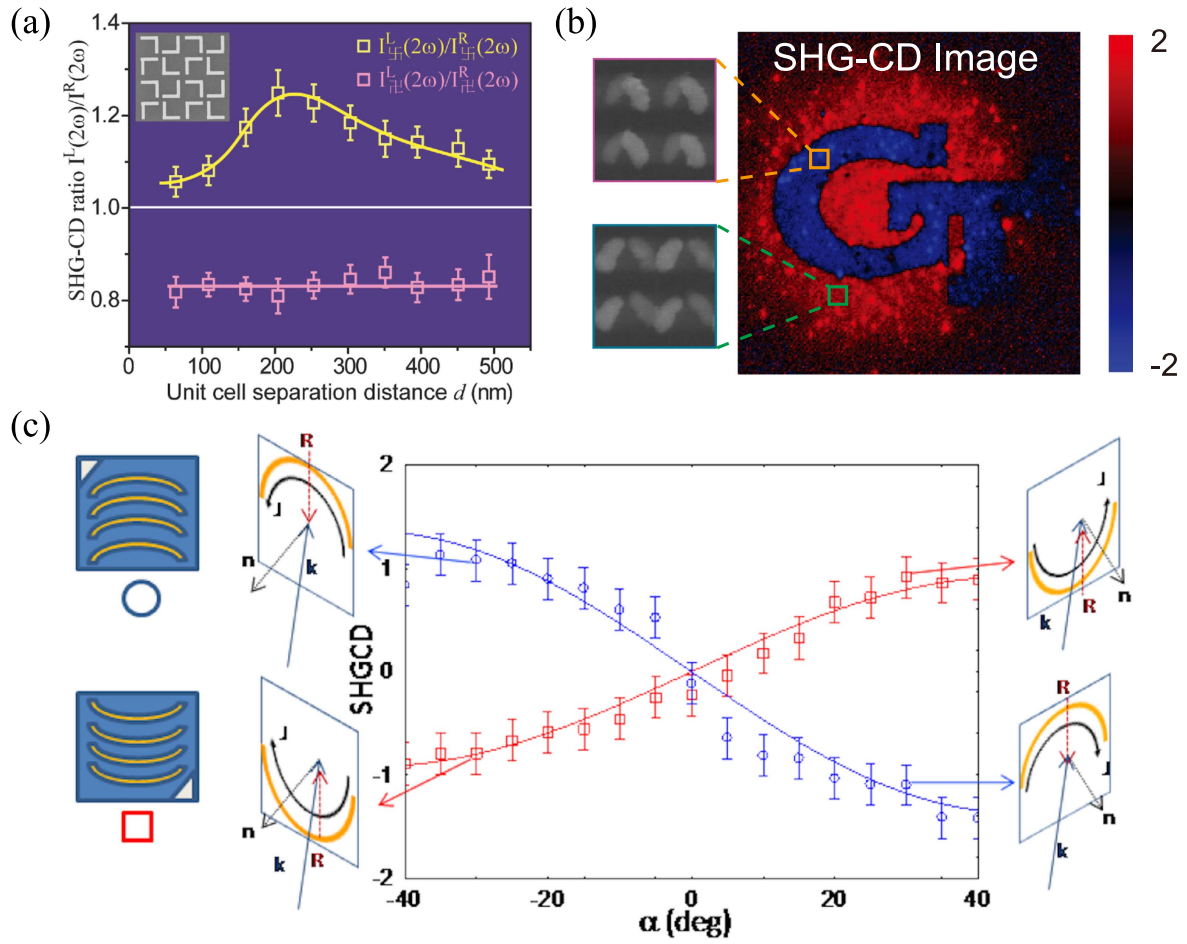

Figure 6. Chiroptical effects in the second-harmonic regime. (a) SHG-CD from two chiral centers (gammadions with opposite handedness) as a function of the gap size. (b) SHG-CD image (right panel) of a 'GT' patterned logo based on twisted-arc structures and the SEM images of the two enantiomers (left panels). (c) SHG-CD of the sample with curved nanowires for 0° (blue circles) and 180° (red squares) orientation of the sample. (a) is adapted from [163], (b) is adapted from [61], and (c) is adapted from [165] with permissions.

in nonlinear light–matter interaction. Specifically, the chiral contrast of the two-photon luminescence was witnessed when a circularly polarized light was incident on the embedded quantum emitters. The two-photon luminescence from the chiral system was remarkably enhanced by over 40× with respect to a reference case without the metamaterials. Moreover, the enhancement was chirality-enabled and was sensitive to the handedness of the illuminations. The enhancement factor for the two spin states achieved a contrast as large as 3 in the experiment. These findings manifest the potential for applications in chiral-selective imaging, sensing, and spectroscopy.

Apart from the enhancement of quantum emitters discussed above, another fascinating application is chirality-selective optoelectronics. In the photoemission process, light absorption in solids can produce hot carriers whose energies are larger than those of thermal excitations at ambient temperatures [171]. Hot carrier science has played an important role in the development of quantum mechanics in the past, and nowadays offers exciting opportunities for fundamental research and applications in optoelectronics, catalysis, and photochemistry. Hot electrons generated from light absorption in a metal can be emitted over a Schottky barrier to produce current. Properly designed plasmonic nanostructures may greatly enhance light absorption and provide valuable control over the emission of the hot electrons in practical applications [172–174]. Chiral plasmonic nanostructures enable disparate light absorption for different circular polarizations and result in chiral-responsive hot-electron devices. To prove this concept, an ultracompact device for circularly polarized light detection has been proposed [175]. As shown in figure 7(b), the designed chiral metamaterial consists of Z-shaped silver stripes on top of a dielectric spacer and an optically thick silver backplane. The chiral metamaterial acts as a perfect LCP light absorber at the resonant wavelength and it reflects nearly 90% of the light of the other spin state. The simulated circular dichrosim (CD = $A_{LCP}-A_{RCP}$) reaches as high as 0.9, promising enhanced discrimination between LCP and RCP in photodetection. In experiment, a Schottky barrier is formed by integrating a semiconductor layer (n-type silicon) on top of the chiral plasmonic structure. Photoresponse spectra match well with the measured absorption spectra, and demonstrate peak photoresponsivity of the resonant state up to 2.2 mA W^{-1}. The corresponding quantum efficiency reaches as high as 0.2%. This efficiency is two times that of chiral organic semiconductor transistors [176].

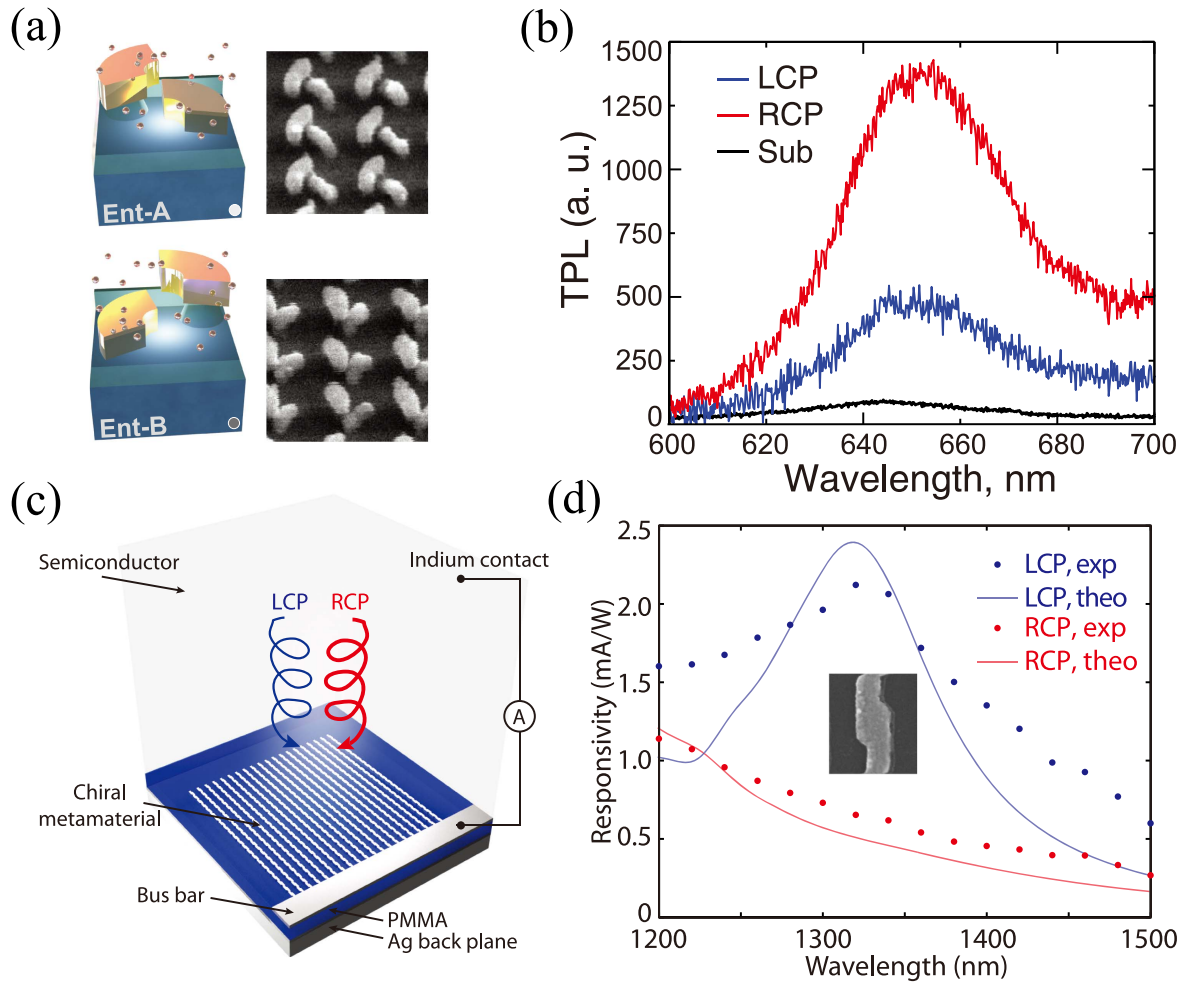

Figure 7. Chiral light–matter interactions. (a) Schematic diagram of enantiomer A (top left) and enantiomer B (bottom left) of the twisted-arc chiral metamaterial. Quantum dots fill the volume mostly surrounding the region around the upper arc. The right panels show the SEM images of two enantiomers. (b) Two-photon luminescence profile at 800 nm under different input circular polarizations for enantiomer A. (c) Schematic diagram of a circular polarized light detector consisting of a chiral metamaterial with a semiconductor that serves as a hot-electron acceptor. (d) Experimentally measured (dots) and theoretically calculated (solid curve) photoresponsivity spectra under LCP (blue) and RCP (red) illumination for left-handed metamaterials. (a) and (b) are adapted from [170], (c) and (d) are adapted from [175] with permissions.

Furthermore, large circular dichroism gives rise to a significant distinction in photocurrents for the two spin states, with a polarization discrimination ratio of 3.4 and a difference in photoresponsivity of 1.5 mA W^{-1}.

5.3. Active chiral metamaterials

Active control over the chirality of metamaterials has the potential of serving as a key element of future optical systems such as polarization sensitive imaging and interactive display. However, achieving active control over chiral metamaterials is challenging since it involves the reconfiguration of the metamolecule from a left-handed enantiomer to a right-handed counterpart and vice versa. In the terahertz regime, the generation of charge carriers via an optical pump in silicon has been utilized to actively switch the overall handedness of chiral structures [177–180]. A pulsed laser working at 800 nm is utilized to excite electron–hole pairs across the 1.12 eV bandgap of silicon. Under the illumination of a 500 mW pump laser, the photoconductivity of silicon can be as high as 50 000 S m^{-1}. This feature enables all-optical switching of the handedness in chiral metamaterials in the THz regime. An all-optical tunable chirality has also been realized in a double-layer metamaterial, which consists of a nonlinear nano-Au: polycrystalline indium-tin oxide layer between two L-shaped nano-antennas in the building block [181]. A 45 nm shift of the peak in the circular dichroism spectrum has been observed under a 40 kW cm^{-2} weak pump. This work opens up the possibility for ultralow-power and ultrafast all-optical tunable chirality at visible frequencies.

Switchable chirality can also be achieved by micro-electro-mechanical systems. In [182], a planar spiral structure is vertically deformed into its three-dimensional counterparts once a pneumatic force is applied (figure 8(a)). The pneumatic force is supplied through air channels with the pressure source of N_2 gas regulated by a pressure injector. Enantiomer switching is realized by selecting the deformation direction, which allows the alteration of the polarity of the optical activity without changing the spectral shape. To eliminate the cross-polarization conversion from birefringence, spiral

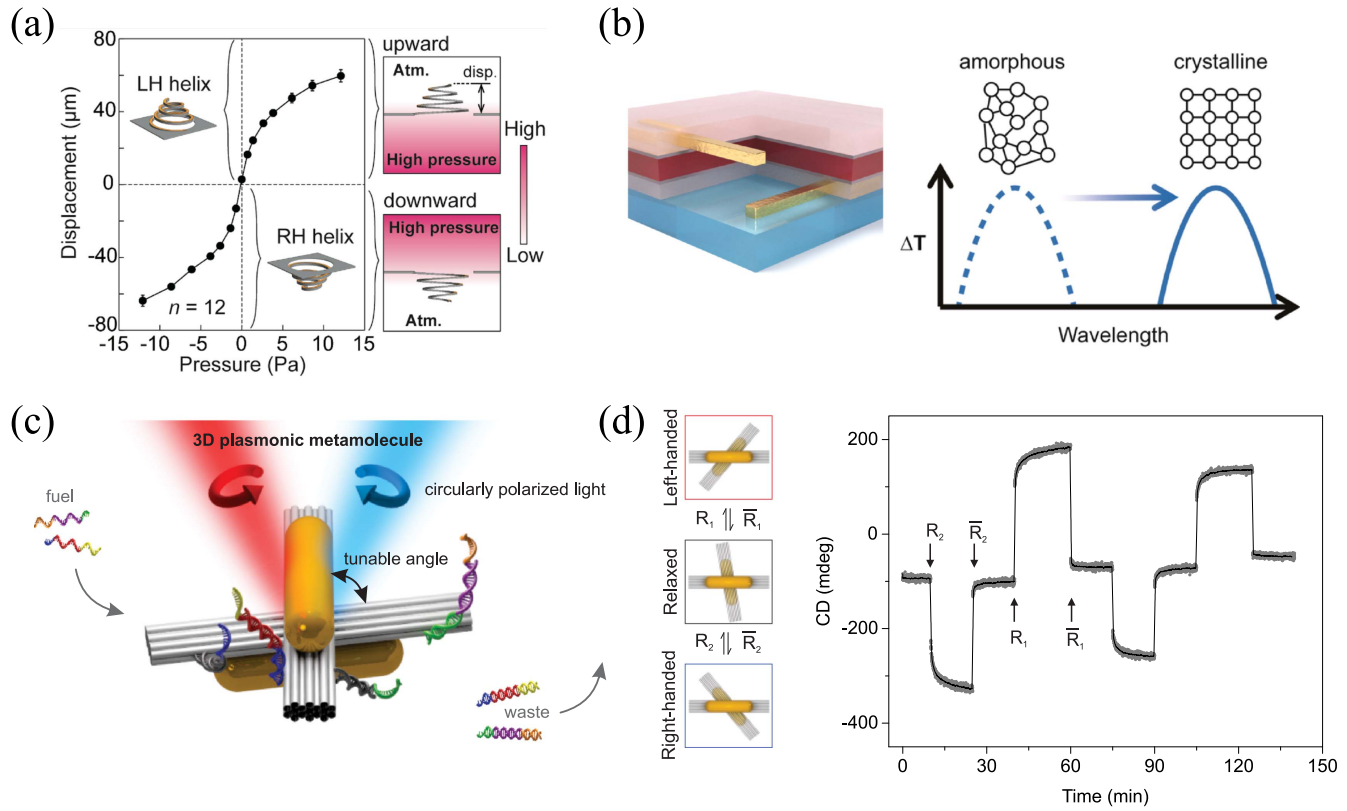

Figure 8. Active chiral metamaterials. (a) Displacement of the spiral structure with respect to the applied pressure of N_2 gas. The sign of the pressure is positive when the pressure is applied to the bottom chamber, resulting in left-handed spirals, and vice versa. (b) Active chiral plasmonic dimer stack consisting of 50 nm GST-326 (red) with two 10 nm ZnS/SiO_2 layers (gray) sandwiched between gold nanorods embedded in PC403 (light red). The right panel depicts the shift of CD signal when the amorphous-to-crystalline phase transition occurs. (c) Schematic diagram of the reconfigurable chiral metamolecules based on DNA self-assembly. Two gold nanorods are hosted on a reconfigurable DNA origami template consisting of two connected bundles, which subtends a tunable angle. (d) Measured CD signals of the plasmonic metamolecules over time at a fixed wavelength of 725 nm. The plasmonic metamolecules can be driven to either handedness by adding removal or return strands. (a) is adapted from [182], (b) is adapted from [189], (c) and (d) are adapted from [192] with permissions.

arrays with C_4 symmetry have been further developed. A polarization rotation of up to 28 degrees has been experimentally observed, which provides a compact polarization modulator in the THz regime.

Phase-change materials [183–186], whose refractive index can be modified by temperature, voltage or light pulses, have been integrated with metamaterials to dynamically control the properties of metamateirals [187, 188]. Very recently, active control of chirality has been experimentally verified in [189], in which a layer of phase-change material $Ge_3Sb_2Te_6$ is sandwiched between two stacked nanorods (figure 8(b)). Such sandwich structures can ensure an optimum interaction between $Ge_3Sb_2Te_6$ and the plasmonic near field, and does not require complex lithography. A thermally induced transition from the amorphous state to the crystalline state occurs when the phase-change layer is heated up to the transition temperature (160 °C), and leads to a change in refractive index from $3.5 + 0.01i$ to $6.5 + 0.06i$. Simulation results demonstrate that a giant spectral shift of around 20% at mid-infrared frequencies occurs when the phase transition happens. The measured circular dichroism spectrum is highly consistent with the theoretical prediction and a large spectral shift of 18% is realized. The wavelength tunability has also been utilized to obtain a reversal in the sign of the circular dichroism. Thermal switching of the handedness at a fixed wavelength is realized by cascading an active right-handed chiral dimer with a passive left-handed one. In the amorphous state, the strong positive CD signals from the active right-handed chiral dimer dominate and make the entire structure right-handed. In the crystalline state, the CD peak red shifts and the signals from the passive left-handed chiral dimer determines the entire chirality of the cascade system. Experiments have demonstrated that for cascade chiral dimers, the CD signal at 4200 nm in the amorphous state is exactly opposite to that in the crystalline state. These findings pave a new way towards thermal-controlled polarization modulation in the mid-infrared region and may find potential applications in thermal imaging and detection.

DNA-directed assembly has recently been proven to be a viable method for the controlled arrangement of plasmonic nanostructures, thus offering reconfigurable chirality [190–192]. As shown in figure 8(c), two gold nanorods are hosted on a reconfigurable DNA template, which consists of two connected bundles folded from a long single-stranded DNA scaffold. The relative angle between nanorods can be controlled by two DNA locks that extended from the sides of the

DNA origami bundles. By adding designed DNA fuel strands, the 3D metamolecules can be switched between different conformational states, thus giving distinct CD spectra. Both of the DNA locks are open in an initially relaxed state. In the left cyclic process, a removal strand is added to dissociate the DNA strand from the arm through a branch migration process. Unreactive waste is produced during this process. The two DNA bundles are joined together, and therefore a left-handed system is established. With the addition of a return strand, the DNA lock is opened again through a second brand migration process. Hence, the system returns to its relax state. Figure 8(d) presents the measured CD signal over time between three distinct states: relaxed, left-handed and right-handed. The wavelength here is fixed at 725 nm. This CD signal clearly describes the cycling between three states of this system. The combination of plasmonics with DNA technology provides a versatile platform for designing active devices and may advance the development of smart probes for life science and biochemistry.

6. Conclusion and outlook

We have seen rapid growth in the field of optical chiral metamaterials, and it will continuously advance. The development of bottom-up and top-down approaches pushes the operation frequency of chiral metamaterials to the THz region and ultimately the optical frequency. Top-down approaches often provide excellent fabrication accuracy and flexibility, yet they are normally costly, low speed and cannot be applied to mass production. The situation is almost reversed in the case of the bottom-up approaches, which are cheaper, faster and regarded as the best methods for mimicking the self-assembly process in real life. We expect that the combination of these two approaches could provide a balance between quality and cost for a promising metamaterial industry. The chiroptical response has been largely discussed in the linear regime, while the nonlinear chiroptical effect in chiral metamaterials is still in its infancy. We expect that a variety of nonlinear processes, such as third harmonic generation, optical rectification and parametric up/down conversion, can provide new routes for the manipulation and utilization of chiroptical responses in either the near or far fields. Judiciously designed plasmonic nanostructures can greatly enhance chiral light–matter interactions, which provide potential opportunities for detecting and characterizing the ubiquitous chirality in nature with unparalleled sensitivity. Although the underlying mechanism and some experimental verification have been demonstrated in several studies highlighted in this review, further fundamental studies are needed to optimize these processes. In particular, it is important to determine what kind of chiral structures are suitable for practical applications. We also expect that more active chiral devices can be produced, reaching dynamic control of not only the far-field chirality but also the near-field counterparts. Last, but not least, since many biologically active molecules and proteins are chiral, we believe that bio-inspired and biocompatible chiral devices with performance that is superior to existing technologies are greatly needed. This in turn will significantly advance developments in biochemistry, biophotonics and other interdisciplinary areas.

Acknowledgments

Z Wang acknowledges the support from China Scholarship Council (201406320105), and Y Liu acknowledges the 3M Non-Tenured Faculty Award.

References

[1] Barron L D 2004 *Molecular Light Scattering and Optical Activity* (New York: Cambridge University Press)
[2] Saranathan V, Osuji C O, Mochrie S G, Noh H, Narayanan S, Sandy A, Dufresne E R and Prum R O 2010 Structure, function, and self-assembly of single network gyroid (I4132) photonic crystals in butterfly wing scales *Proc. Natl Acad. Sci. USA* **107** 11676–81
[3] Sharma V, Crne M, Park J O and Srinivasarao M 2009 Structural origin of circularly polarized iridescence in jeweled beetles *Science* **325** 449–51
[4] Smith D R, Pendry J B and Wiltshire M C K 2004 Metamaterials and negative refractive index *Science* **305** 788–92
[5] Liu Y and Zhang X 2011 Metamaterials: a new frontier of science and technology *Chem. Soc. Rev.* **40** 2494–507
[6] Soukoulis C M and Wegener M 2011 Past achievements and future challenges in the development of three-dimensional photonic metamaterials *Nat. Photon.* **5** 523–30
[7] Cai W and Shalaev V M 2010 *Optical Metamaterials: Fundamentals and Applications* vol 10 (New York: Springer)
[8] Pendry J B, Holden A J, Stewart W J and Youngs I 1996 Extremely low frequency plasmons in metallic mesostructures *Phys. Rev. Lett.* **76** 4773–6
[9] Pendry J B, Holden A J, Robbins D J and Stewart W J 1999 Magnetism from conductors and enhanced nonlinear phenomena *IEEE Trans. Microwave Theory Tech.* **47** 2075–84
[10] Smith D R and Kroll N 2000 Negative refractive index in left-handed materials *Phys. Rev. Lett.* **85** 2933–6
[11] Pendry J B 2000 Negative refraction makes a perfect lens *Phys. Rev. Lett.* **85** 3966–9
[12] Fang N, Lee H, Sun C and Zhang X 2005 Sub–diffraction-limited optical imaging with a silver superlens *Science* **308** 534–7
[13] Zhang X and Liu Z W 2008 Superlenses to overcome the diffraction limit *Nat. Mater.* **7** 435–41
[14] Pendry J B, Schurig D and Smith D R 2006 Controlling electromagnetic fields *Science* **312** 1780–2
[15] Leonhardt U 2006 Optical conformal mapping *Science* **312** 1777–80
[16] Li J and Pendry J 2008 Hiding under the carpet: a new strategy for cloaking *Phys. Rev. Lett.* **101** 203901
[17] Valentine J, Li J S, Zentgraf T, Bartal G and Zhang X 2009 An optical cloak made of dielectrics *Nat. Mater.* **8** 568–71
[18] Landy N and Smith D R 2013 A full-parameter unidirectional metamaterial cloak for microwaves *Nat. Mater.* **12** 25–8
[19] Lai Y, Ng J, Chen H Y, Han D Z, Xiao J J, Zhang Z Q and Chan C T 2009 Illusion optics: the optical transformation of an object into another object *Phys. Rev. Lett.* **102** 253902

[20] Shelby R A, Smith D R and Schultz S 2001 Experimental verification of a negative index of refraction *Science* **292** 77–9

[21] Smith D R, Padilla W J, Vier D C, Nemat-Nasser S C and Schultz S 2000 Composite medium with simultaneously negative permeability and permittivity *Phys. Rev. Lett.* **84** 4184–7

[22] Zhang S, Fan W, Malloy K J, Brueck S R J, Panoiu N C and Osgood R M 2005 Near-infrared double negative metamaterials *Opt. Express* **13** 4922–30

[23] Valentine J, Zhang S, Zentgraf T, Ulin-Avila E, Genov D A, Bartal G and Zhang X 2008 Three-dimensional optical metamaterial with a negative refractive index *Nature* **455** 376–9

[24] Chen H, Wang Z, Zhang R, Wang H, Lin S, Yu F and Moser H O 2014 A meta-substrate to enhance the bandwidth of metamaterials *Sci. Rep.* **4** 5264

[25] Tretyakov S, Nefedov I, Sihvola A, Maslovski S and Simovski C 2003 Waves and energy in chiral nihility *J. Electromagn. Waves Appl.* **17** 695–706

[26] Pendry J B 2004 A chiral route to negative refraction *Science* **306** 1353–5

[27] Monzon C and Forester D W 2005 Negative refraction and focusing of circularly polarized waves in optically active media *Phys. Rev. Lett.* **95** 123904

[28] Plum E, Zhou J, Dong J, Fedotov V A, Koschny T, Soukoulis C M and Zheludev N I 2009 Metamaterial with negative index due to chirality *Phys. Rev.* B **79** 035407

[29] Rogacheva A V, Fedotov V A, Schwanecke A S and Zheludev N I 2006 Giant gyrotropy due to electromagnetic-field coupling in a bilayered chiral structure *Phys. Rev. Lett.* **97** 177401

[30] Zhou J, Dong J, Wang B, Koschny T, Kafesaki M and Soukoulis C M 2009 Negative refractive index due to chirality *Phys. Rev.* B **79** 121104

[31] Zhang S, Park Y-S, Li J, Lu X, Zhang W and Zhang X 2009 Negative refractive index in chiral metamaterials *Phys. Rev. Lett.* **102** 023901

[32] Plum E, Fedotov V A, Schwanecke A S, Zheludev N I and Chen Y 2007 Giant optical gyrotropy due to electromagnetic coupling *Appl. Phys. Lett.* **90** 223113

[33] Decker M, Klein M W, Wegener M and Linden S 2007 Circular dichroism of planar chiral magnetic metamaterials *Opt. Lett.* **32** 856–8

[34] Kuwata-Gonokami M, Saito N, Ino Y, Kauranen M, Jefimovs K, Vallius T, Turunen J and Svirko Y 2005 Giant optical activity in quasi-two-dimensional planar nanostructures *Phys. Rev. Lett.* **95** 227401

[35] Wang B, Zhou J, Koschny T and Soukoulis C M 2009 Nonplanar chiral metamaterials with negative index *Appl. Phys. Lett.* **94** 151112

[36] Bingnan W, Jiangfeng Z, Thomas K, Maria K and Costas M S 2009 Chiral metamaterials: simulations and experiments *J. Opt. A: Pure Appl. Opt.* **11** 114003

[37] Li Z, Mutlu M and Ozbay E 2013 Chiral metamaterials: from optical activity and negative refractive index to asymmetric transmission *J. Opt.* **15** 023001

[38] Gansel J K, Thiel M, Rill M S, Decker M, Bade K, Saile V, von Freymann G, Linden S and Wegener M 2009 Gold helix photonic metamaterial as broadband circular polarizer *Science* **325** 1513–5

[39] Menzel C, Helgert C, Rockstuhl C, Kley E B, Tünnermann A, Pertsch T and Lederer F 2010 Asymmetric transmission of linearly polarized light at optical metamaterials *Phys. Rev. Lett.* **104** 253902

[40] Fedotov V A, Schwanecke A S, Zheludev N I, Khardikov V V and Prosvirnin S L 2007 Asymmetric transmission of light and enantiomerically sensitive plasmon resonance in planar chiral nanostructures *Nano Lett.* **7** 1996–9

[41] Schwanecke A S, Fedotov V A, Khardikov V V, Prosvirnin S L, Chen Y and Zheludev N I 2008 Nanostructured metal film with asymmetric optical transmission *Nano Lett.* **8** 2940–3

[42] Fedotov V A, Mladyonov P L, Prosvirnin S L, Rogacheva A V, Chen Y and Zheludev N I 2006 Asymmetric propagation of electromagnetic waves through a planar chiral structure *Phys. Rev. Lett.* **97** 167401

[43] Schäferling M, Dregely D, Hentschel M and Giessen H 2012 Tailoring enhanced optical chirality: design principles for chiral plasmonic nanostructures *Phys. Rev. X* **2** 031010

[44] Smith D R, Schultz S, Markoš P and Soukoulis C M 2002 Determination of effective permittivity and permeability of metamaterials from reflection and transmission coefficients *Phys. Rev.* B **65** 195104

[45] Chen X, Wu B-I, Kong J A and Grzegorczyk T M 2005 Retrieval of the effective constitutive parameters of bianisotropic metamaterials *Phys. Rev.* E **71** 046610

[46] Zhao R, Koschny T and Soukoulis C M 2010 Chiral metamaterials: retrieval of the effective parameters with and without substrate *Opt. Express* **18** 14553–67

[47] Menzel C, Paul T, Rockstuhl C, Pertsch T, Tretyakov S and Lederer F 2010 Validity of effective material parameters for optical fishnet metamaterials *Phys. Rev.* B **81** 035320

[48] Simovski C R and Tretyakov S A 2010 On effective electromagnetic parameters of artificial nanostructured magnetic materials *Photonoics Nanostruct. Fundam. Appl.* **8** 254–63

[49] Jones R C 1941 A new calculus for the treatment of optical systemsi. description and discussion of the calculus *J. Opt. Soc. Am.* **31** 488–93

[50] Menzel C, Rockstuhl C and Lederer F 2010 Advanced Jones calculus for the classification of periodic metamaterials *Phys. Rev.* A **82** 053811

[51] Potton R J 2004 Reciprocity in optics *Rep. Prog. Phys.* **67** 717

[52] Kaschke J, Gansel J K and Wegener M 2012 On metamaterial circular polarizers based on metal N-helices *Opt. Express* **20** 26012–20

[53] Kaschke J, Blome M, Burger S and Wegener M 2014 Tapered N-helical metamaterials with three-fold rotational symmetry as improved circular polarizers *Opt. Express* **22** 19936–46

[54] Kwon D-H, Werner D H, Kildishev A V and Shalaev V M 2008 Material parameter retrieval procedure for general bi-isotropic metamaterials and its application to optical chiral negative-index metamaterial design *Opt. Express* **16** 11822–9

[55] Saba M, Turner M D, Mecke K, Gu M and Schröder-Turk G E 2013 Group theory of circular-polarization effects in chiral photonic crystals with four-fold rotation axes applied to the eight-fold intergrowth of gyroid nets *Phys. Rev.* B **88** 245116

[56] Plum E, Fedotov V A and Zheludev N I 2009 Planar metamaterial with transmission and reflection that depend on the direction of incidence *Appl. Phys. Lett.* **94** 131901

[57] Kenanakis G, Xomalis A, Selimis A, Vamvakaki M, Farsari M, Kafesaki M, Soukoulis C M and Economou E N 2015 Three-dimensional infrared metamaterial with asymmetric transmission *ACS Photonics* **2** 287–94

[58] Ma X, Huang C, Pu M, Hu C, Feng Q and Luo X 2012 Multi-band circular polarizer using planar spiral metamaterial structure *Opt. Express* **20** 16050–8

[59] Ma X, Huang C, Pu M, Wang Y, Zhao Z, Wang C and Luo X 2012 Dual-band asymmetry chiral metamaterial based on planar spiral structure *Appl. Phys. Lett.* **101** 161901

[60] Cui Y H, Kang L, Lan S F, Rodrigues S and Cai W S 2014 Giant chiral optical response from a twisted-arc metamaterial *Nano Lett.* **14** 1021–5

[61] Rodrigues S P, Lan S, Kang L, Cui Y and Cai W 2014 Nonlinear imaging and spectroscopy of chiral metamaterials *Adv. Mater.* **26** 6157–62

[62] Yu N and Capasso F 2014 Flat optics with designer metasurfaces *Nat. Mater.* **13** 139–50

[63] Huang L L, Chen X Z, Muhlenbernd H, Li G X, Bai B F, Tan Q F, Jin G F, Zentgraf T and Zhang S 2012 Dispersionless phase discontinuities for controlling light propagation *Nano Lett.* **12** 5750–5

[64] Ma X, Pu M, Li X, Huang C, Wang Y, Pan W, Zhao B, Cui J, Wang C and Zhao Z 2015 A planar chiral meta-surface for optical vortex generation and focusing *Sci. Rep.* **5** 10365

[65] Shaltout A, Liu J, Shalaev V M and Kildishev A V 2014 Optically active metasurface with non-chiral plasmonic nanoantennas *Nano Lett.* **14** 4426–31

[66] Lin D, Fan P, Hasman E and Brongersma M L 2014 Dielectric gradient metasurface optical elements *Science* **345** 298–302

[67] Pu M, Li X, Ma X, Wang Y, Zhao Z, Wang C, Hu C, Gao P, Huang C and Ren H 2015 Catenary optics for achromatic generation of perfect optical angular momentum *Sci. Adv.* **1** e1500396

[68] Zheng G, Muhlenbernd H, Kenney M, Li G, Zentgraf T and Zhang S 2015 Metasurface holograms reaching 80% efficiency *Nat. Nanotechnol.* **10** 308–12

[69] Gansel J K, Latzel M, Frölich A, Kaschke J, Thiel M and Wegener M 2012 Tapered gold-helix metamaterials as improved circular polarizers *Appl. Phys. Lett.* **100** 101109

[70] Thiel M, Rill M S, von Freymann G and Wegener M 2009 Three-dimensional Bi-chiral photonic crystals *Adv. Mater.* **21** 4680–2

[71] Radke A, Gissibl T, Klotzbücher T, Braun P V and Giessen H 2011 Three-dimensional bichiral plasmonic crystals fabricated by direct laser writing and electroless silver plating *Adv. Mater.* **23** 3018–21

[72] Yeom B, Zhang H, Zhang H, Park J I, Kim K, Govorov A O and Kotov N A 2013 Chiral plasmonic nanostructures on achiral nanopillars *Nano Lett.* **13** 5277–83

[73] Larsen G K, He Y, Ingram W and Zhao Y 2013 Hidden chirality in superficially racemic patchy silver films *Nano Lett.* **13** 6228–32

[74] Mark A G, Gibbs J G, Lee T-C and Fischer P 2013 Hybrid nanocolloids with programmed three-dimensional shape and material composition *Nat. Mater.* **12** 802–7

[75] Singh J H, Nair G, Ghosh A and Ghosh A 2013 Wafer scale fabrication of porous three-dimensional plasmonic metamaterials for the visible region: chiral and beyond *Nanoscale* **5** 7224–8

[76] Gibbs J G, Mark A G, Eslami S and Fischer P 2013 Plasmonic nanohelix metamaterials with tailorable giant circular dichroism *Appl. Phys. Lett.* **103** 213101

[77] Frank B, Yin X, Schäferling M, Zhao J, Hein S M, Braun P V and Giessen H 2013 Large-area 3D chiral plasmonic structures *ACS Nano* **7** 6321–9

[78] Dietrich K, Lehr D, Helgert C, Tünnermann A and Kley E-B 2012 Circular dichroism from chiral nanomaterial fabricated by on-edge lithography *Adv. Mater.* **24** OP321–5

[79] Esposito M, Tasco V, Todisco F, Benedetti A, Sanvitto D and Passaseo A 2014 Three dimensional chiral metamaterial nanospirals in the visible range by vertically compensated focused ion beam induced-deposition *Adv. Opt. Mater* **2** 154–61

[80] Esposito M, Tasco V, Todisco F, Cuscunà M, Benedetti A, Sanvitto D and Passaseo A 2015 Triple-helical nanowires by tomographic rotatory growth for chiral photonics *Nat. Commun.* **6** 6484

[81] Koops H W P, Kretz J, Rudolph M and Weber M 1993 Constructive three-dimensional lithography with electron-beam induced deposition for quantum effect devices *J. Vac. Sci. Technol.* B **11** 2386–9

[82] Utke I, Hoffmann P and Melngailis J 2008 Gas-assisted focused electron beam and ion beam processing and fabrication *J. Vac. Sci. Technol.* B **26** 1197–276

[83] van Dorp W F and Hagen C W 2008 A critical literature review of focused electron beam induced deposition *J. Appl. Phys.* **104** 081301

[84] Esposito M, Tasco V, Cuscunà M, Todisco F, Benedetti A, Tarantini I, Giorgi M D, Sanvitto D and Passaseo A 2015 Nanoscale 3D chiral plasmonic helices with circular dichroism at visible frequencies *ACS Photonics* **2** 105–14

[85] Liu N, Liu H, Zhu S and Giessen H 2009 Stereometamaterials *Nat. Photon.* **3** 157–62

[86] Haken H and Wolf H C 2004 *Molecular Physics and Elements of Quantum Chemistry* (Berlin: Springer)

[87] Hentschel M, Schäferling M, Weiss T, Liu N and Giessen H 2012 Three-dimensional chiral plasmonic oligomers *Nano Lett.* **12** 2542–7

[88] Hentschel M, Wu L, Schäferling M, Bai P, Li E P and Giessen H 2012 Optical properties of chiral three-dimensional plasmonic oligomers at the onset of charge-transfer plasmons *ACS Nano* **6** 10355–65

[89] Hentschel M, Schäferling M, Metzger B and Giessen H 2013 Plasmonic diastereomers: adding up chiral centers *Nano Lett.* **13** 600–6

[90] Helgert C, Pshenay-Severin E, Falkner M, Menzel C, Rockstuhl C, Kley E-B, Tünnermann A, Lederer F and Pertsch T 2011 Chiral metamaterial composed of three-dimensional plasmonic nanostructures *Nano Lett.* **11** 4400–4

[91] Decker M, Ruther M, Kriegler C E, Zhou J, Soukoulis C M, Linden S and Wegener M 2009 Strong optical activity from twisted-cross photonic metamaterials *Opt. Lett.* **34** 2501–3

[92] Liu N and Giessen H 2008 Three-dimensional optical metamaterials as model systems for longitudinal and transverse magnetic coupling *Opt. Express* **16** 21233–8

[93] Xiong X, Sun W-H, Bao Y-J, Wang M, Peng R-W, Sun C, Lu X, Shao J, Li Z-F and Ming N-B 2010 Construction of a chiral metamaterial with a U-shaped resonator assembly *Phys. Rev.* B **81** 075119

[94] Kenanakis G, Zhao R, Stavrinidis A, Konstantinidis G, Katsarakis N, Kafesaki M, Soukoulis C and Economou E 2012 Flexible chiral metamaterials in the terahertz regime: a comparative study of various designs *Optical Materials Express* **2** 1702–12

[95] Zhao Y, Belkin M A and Alù A 2012 Twisted optical metamaterials for planarized ultrathin broadband circular polarizers *Nat. Commun.* **3** 870

[96] Karimullah A S, Jack C, Tullius R, Rotello V M, Cooke G, Gadegaard N, Barron L D and Kadodwala M 2015 Disposable plasmonics: plastic templated plasmonic metamaterials with tunable chirality *Adv. Mater.* **27** 5610–6

[97] Min Y, Akbulut M, Kristiansen K, Golan Y and Israelachvili J 2008 The role of interparticle and external forces in nanoparticle assembly *Nat. Mater.* **7** 527–38

[98] Bishop K J M, Wilmer C E, Soh S and Grzybowski B A 2009 Nanoscale forces and their uses in self-assembly *Small* **5** 1600–30

[99] Petty J T, Zheng J, Hud N V and Dickson R M 2004 DNA-templated Ag nanocluster formation *J. Am. Chem. Soc.* **126** 5207–12

[100] Shemer G, Krichevski O, Markovich G, Molotsky T, Lubitz I and Kotlyar A B 2006 Chirality of silver nanoparticles synthesized on DNA *J. Am. Chem. Soc.* **128** 11006–7

[101] Mastroianni A J, Claridge S A and Alivisatos A P 2009 Pyramidal and chiral groupings of gold nanocrystals

assembled using DNA scaffolds *J. Am. Chem. Soc.* **131** 8455–9
[102] Yan W, Xu L, Xu C, Ma W, Kuang H, Wang L and Kotov N A 2012 Self-assembly of chiral nanoparticle pyramids with strong R/S optical activity *J. Am. Chem. Soc.* **134** 15114–21
[103] Fan Z, Zhang H and Govorov A O 2013 Optical properties of chiral plasmonic tetramers: circular dichroism and multipole effects *J. Phys. Chem.* C **117** 14770–7
[104] Ferry V E, Smith J M and Alivisatos A P 2014 Symmetry breaking in tetrahedral chiral plasmonic nanoparticle assemblies *ACS Photonics* **1** 1189–96
[105] Lan X, Chen Z, Dai G, Lu X, Ni W and Wang Q 2013 Bifacial DNA origami-directed discrete, three-dimensional, anisotropic plasmonic nanoarchitectures with tailored optical chirality *J. Am. Chem. Soc.* **135** 11441–4
[106] Shen X, Asenjo-Garcia A, Liu Q, Jiang Q, García de Abajo F J, Liu N and Ding B 2013 Three-dimensional plasmonic chiral tetramers assembled by DNA origami *Nano Lett.* **13** 2128–33
[107] Ma W *et al* 2013 Chiral plasmonics of self-assembled nanorod dimers *Sci. Rep.* **3** 1934
[108] Rothemund P W K 2006 Folding DNA to create nanoscale shapes and patterns *Nature* **440** 297–302
[109] Douglas S M, Dietz H, Liedl T, Hogberg B, Graf F and Shih W M 2009 Self-assembly of DNA into nanoscale three-dimensional shapes *Nature* **459** 414–8
[110] Sharma J, Chhabra R, Cheng A, Brownell J, Liu Y and Yan H 2009 Control of self-assembly of DNA tubules through integration of gold nanoparticles *Science* **323** 112–6
[111] Sharma J, Chhabra R, Andersen C S, Gothelf K V, Yan H and Liu Y 2008 Toward reliable gold nanoparticle patterning on self-assembled DNA nanoscaffold *J. Am. Chem. Soc.* **130** 7820–1
[112] Shen X, Song C, Wang J, Shi D, Wang Z, Liu N and Ding B 2012 Rolling up gold nanoparticle-dressed DNA origami into three-dimensional plasmonic chiral nanostructures *J. Am. Chem. Soc.* **134** 146–9
[113] Kuzyk A, Schreiber R, Fan Z, Pardatscher G, Roller E-M, Hogele A, Simmel F C, Govorov A O and Liedl T 2012 DNA-based self-assembly of chiral plasmonic nanostructures with tailored optical response *Nature* **483** 311–4
[114] Chen Z, Lan X, Chiu Y-C, Lu X, Ni W, Gao H and Wang Q 2015 Strong chiroptical activities in gold nanorod dimers assembled using DNA origami templates *ACS Photonics* **2** 392–7
[115] Li Y G and Liu M H 2008 Fabrication of chiral silver nanoparticles and chiral nanoparticulate film via organogel *Chem. Commun.* 5571–3
[116] Zhu Z, Liu W, Li Z, Han B, Zhou Y, Gao Y and Tang Z 2012 Manipulation of collective optical activity in one-dimensional plasmonic assembly *ACS Nano* **6** 2326–32
[117] Chen C-L, Zhang P and Rosi N L 2008 A new peptide-based method for the design and synthesis of nanoparticle superstructures: construction of highly ordered gold nanoparticle double helices *J. Am. Chem. Soc.* **130** 13555–7
[118] Chen C-L and Rosi N L 2010 Preparation of unique 1D nanoparticle superstructures and tailoring their structural features *J. Am. Chem. Soc.* **132** 6902–3
[119] Song C, Blaber M G, Zhao G, Zhang P, Fry H C, Schatz G C and Rosi N L 2013 Tailorable plasmonic circular dichroism properties of helical nanoparticle superstructures *Nano Lett.* **13** 3256–61
[120] Querejeta-Fernández A, Chauve G, Methot M, Bouchard J and Kumacheva E 2014 Chiral plasmonic films formed by gold nanorods and cellulose nanocrystals *J. Am. Chem. Soc.* **136** 4788–93
[121] Thérien-Aubin H, Lukach A, Pitch N and Kumacheva E 2015 Coassembly of nanorods and nanospheres in suspensions and in stratified films *Angew. Chem.* **127** 5710–4
[122] Chu G, Wang X, Chen T, Gao J, Gai F, Wang Y and Xu Y 2015 Optically tunable chiral plasmonic guest–host cellulose films weaved with long-range ordered silver nanowires *ACS Appl. Mater. Interfaces* **7** 11863–70
[123] Querejeta-Fernández A, Kopera B, Prado K S, Klinkova A, Methot M, Chauve G, Bouchard J, Helmy A S and Kumacheva E 2015 Circular dichroism of chiral nematic films of cellulose nanocrystals loaded with plasmonic nanoparticles *ACS Nano* **9** 10377–85
[124] Bitar R, Agez G and Mitov M 2011 Cholesteric liquid crystal self-organization of gold nanoparticles *Soft Matter* **7** 8198–206
[125] Wang R-Y, Wang H, Wu X, Ji Y, Wang P, Qu Y and Chung T-S 2011 Chiral assembly of gold nanorods with collective plasmonic circular dichroism response *Soft Matter* **7** 8370–5
[126] Ayeb H, Grand J, Sellame H, Truong S, Aubard J, Felidj N, Mlayah A and Lacaze E 2012 Gold nanoparticles in a cholesteric liquid crystal matrix: self-organization and localized surface plasmon properties *J. Mater. Chem.* **22** 7856–62
[127] Wang X, Zou Y, Zhu J and Wang Y 2013 Silver cholesteric liquid crystalline: shape-dependent assembly and plasmonic chiroptical response *J. Phys. Chem.* C **117** 14197–205
[128] Infusino M, De Luca A, Ciuchi F, Ionescu A, Scaramuzza N and Strangi G 2013 Effects of gold nanoparticle dispersion in a chiral liquid crystal matrix *Mol. Cryst. Liq. Cryst.* **572** 59–65
[129] Che S, Liu Z, Ohsuna T, Sakamoto K, Terasaki O and Tatsumi T 2004 Synthesis and characterization of chiral mesoporous silica *Nature* **429** 281–4
[130] Xie J and Che S 2012 Chirality of anisotropic metal nanowires with a distinct multihelix *Chem. Eur. J.* **18** 15954–9
[131] Guerrero-Martínez A, Auguié B, Alonso-Gómez J L, Džolić Z, Gómez-Graña S, Žinić M, Cid M M and Liz-Marzán L M 2011 Intense optical activity from three-dimensional chiral ordering of plasmonic nanoantennas *Angew. Chem. Int. Ed.* **50** 5499–503
[132] Vignolini S, Yufa N A, Cunha P S, Guldin S, Rushkin I, Stefik M, Hur K, Wiesner U, Baumberg J J and Steiner U 2012 A 3D optical metamaterial made by self-assembly *Adv. Mater.* **24** OP23–7
[133] Salvatore S, Demetriadou A, Vignolini S, Oh S S, Wuestner S, Yufa N A, Stefik M, Wiesner U, Baumberg J J and Hess O 2013 Tunable 3D extended self-assembled gold metamaterials with enhanced light transmission *Adv. Mater.* **25** 2713–6
[134] Slocik J M, Govorov A O and Naik R R 2011 Plasmonic circular dichroism of peptide-functionalized gold nanoparticles *Nano Lett.* **11** 701–5
[135] Behar-Levy H, Neumann O, Naaman R and Avnir D 2007 Chirality induction in bulk gold and silver *Adv. Mater.* **19** 1207–11
[136] Lieberman I, Shemer G, Fried T, Kosower E M and Markovich G 2008 Plasmon-resonance-enhanced absorption and circular dichroism *Angew. Chem. Int. Ed.* **47** 4855–7
[137] Song C, Wang Y and Rosi N L 2013 Peptide-directed synthesis and assembly of hollow spherical copt nanoparticle superstructures *Angew. Chem. Int. Ed.* **52** 3993–5
[138] Williams R 1968 Optical rotatory effect in the nematic liquid phase of p-azoxyanisole *Phys. Rev. Lett.* **21** 342
[139] Plum E, Liu X X, Fedotov V A, Chen Y, Tsai D P and Zheludev N I 2009 Metamaterials: optical activity without chirality *Phys. Rev. Lett.* **102** 113902

[140] Yokoyama A, Yoshida M, Ishii A and Kato Y 2014 Giant circular dichroism in individual carbon nanotubes induced by extrinsic chirality *Phys. Rev.* X **4** 011005

[141] Rizza C, Di Falco A, Scalora M and Ciattoni A 2015 One-dimensional chirality: strong optical activity in epsilon-near-zero metamaterials *Phys. Rev. Lett.* **115** 057401

[142] Ogier R, Fang Y, Käll M and Svedendahl M 2015 Near-complete photon spin selectivity in a metasurface of anisotropic plasmonic antennas *Phys. Rev.* X **5** 041019

[143] Fasman G D 1996 *Circular Dichroism and the Conformational Analysis of Biomolecules* (New York: Springer)

[144] Valev V, Smisdom N, Silhanek A, De Clercq B, Gillijns W, Ameloot M, Moshchalkov V and Verbiest T 2009 Plasmonic ratchet wheels: switching circular dichroism by arranging chiral nanostructures *Nano Lett.* **9** 3945–8

[145] Hendry E, Carpy T, Johnston J, Popland M, Mikhaylovskiy R, Lapthorn A, Kelly S, Barron L, Gadegaard N and Kadodwala M 2010 Ultrasensitive detection and characterization of biomolecules using superchiral fields *Nat. Nanotechnol.* **5** 783–7

[146] Govorov A O, Fan Z, Hernandez P, Slocik J M and Naik R R 2010 Theory of circular dichroism of nanomaterials comprising chiral molecules and nanocrystals: plasmon enhancement, dipole interactions, and dielectric effects *Nano Lett.* **10** 1374–82

[147] Govorov A O 2011 Plasmon-induced circular dichroism of a chiral molecule in the vicinity of metal nanocrystals. application to various geometries *J. Phys. Chem.* C **115** 7914–23

[148] Gerard V A, Gun'ko Y K, Defrancq E and Govorov A O 2011 Plasmon-induced CD response of oligonucleotide-conjugated metal nanoparticles *Chem. Commun.* **47** 7383–5

[149] Lipkin D M 1964 Existence of a new conservation law in electromagnetic theory *J. Math. Phys.* **5** 696–700

[150] Tang Y and Cohen A E 2011 Enhanced enantioselectivity in excitation of chiral molecules by superchiral light *Science* **332** 333–6

[151] Tang Y and Cohen A E 2010 Optical chirality and its interaction with matter *Phys. Rev. Lett.* **104** 163901

[152] Craig D and Thirunamachandran T 1999 New approaches to chiral discrimination in coupling between molecules *Theor. Chem. Acc.* **102** 112–20

[153] Hendry E, Mikhaylovskiy R, Barron L, Kadodwala M and Davis T 2012 Chiral electromagnetic fields generated by arrays of nanoslits *Nano Lett.* **12** 3640–4

[154] Schäferling M, Yin X and Giessen H 2012 Formation of chiral fields in a symmetric environment *Opt. Express* **20** 26326–36

[155] Davis T and Hendry E 2013 Superchiral electromagnetic fields created by surface plasmons in nonchiral metallic nanostructures *Phys. Rev.* B **87** 085405

[156] Petralli-Mallow T, Wong T, Byers J, Yee H and Hicks J 1993 Circular dichroism spectroscopy at interfaces: a surface second harmonic generation study *J. Phys. Chem.* **97** 1383–8

[157] Byers J, Yee H, Petralli-Mallow T and Hicks J 1994 Second-harmonic generation circular-dichroism spectroscopy from chiral monolayers *Phys. Rev.* B **49** 14643

[158] Fischer P and Hache F 2005 Nonlinear optical spectroscopy of chiral molecules *Chirality* **17** 421–37

[159] Boyd R W 2003 *Nonlinear Optics* (San Diego, CA: Academic Press)

[160] Valev V, Silhanek A, Smisdom N, De Clercq B, Gillijns W, Aktsipetrov O, Ameloot M, Moshchalkov V and Verbiest T 2010 Linearly polarized second harmonic generation microscopy reveals chirality *Opt. Express* **18** 8286–93

[161] Valev V, Silhanek A, Verellen N, Gillijns W, Van Dorpe P, Aktsipetrov O, Vandenbosch G, Moshchalkov V and Verbiest T 2010 Asymmetric optical second-harmonic generation from chiral G-shaped gold nanostructures *Phys. Rev. Lett.* **104** 127401

[162] Huttunen M J, Bautista G, Decker M, Linden S, Wegener M and Kauranen M 2011 Nonlinear chiral imaging of subwavelength-sized twisted-cross gold nanodimers *Opt. Mater. Express* **1** 46–56

[163] Valev V K, Baumberg J, De Clercq B, Braz N, Zheng X, Osley E, Vandendriessche S, Hojeij M, Blejean C and Mertens J 2014 Nonlinear superchiral meta-surfaces: tuning chirality and disentangling non-reciprocity at the nanoscale *Adv. Mater.* **26** 4074–81

[164] Verbiest T, Kauranen M, Van Rompaey Y and Persoons A 1996 Optical activity of anisotropic achiral surfaces *Phys. Rev. Lett.* **77** 1456

[165] Belardini A, Larciprete M, Centini M, Fazio E, Sibilia C, Chiappe D, Martella C, Toma A, Giordano M and de Mongeot F B 2011 Circular dichroism in the optical second-harmonic emission of curved gold metal nanowires *Phys. Rev. Lett.* **107** 257401

[166] García-Etxarri A and Dionne J A 2013 Surface-enhanced circular dichroism spectroscopy mediated by nonchiral nanoantennas *Phys. Rev.* B **87** 235409

[167] Yoo S, Cho M and Park Q-H 2014 Globally enhanced chiral field generation by negative-index metamaterials *Phys. Rev.* B **89** 161405

[168] Yoo S and Park Q-H 2015 Chiral light–matter interaction in optical resonators *Phys. Rev. Lett.* **114** 203003

[169] Alaeian H and Dionne J A 2015 Controlling electric, magnetic, and chiral dipolar emission with PT-symmetric potentials *Phys. Rev.* B **91** 245108

[170] Rodrigues S P, Cui Y, Lan S, Kang L and Cai W 2015 Metamaterials enable chiral-selective enhancement of two-photon luminescence from quantum emitters *Adv. Mater.* **27** 1124–30

[171] Brongersma M L, Halas N J and Nordlander P 2015 Plasmon-induced hot carrier science and technology *Nat. Nanotechnol.* **10** 25–34

[172] Chalabi H, Schoen D and Brongersma M L 2014 Hot-electron photodetection with a plasmonic nanostripe antenna *Nano Lett.* **14** 1374–80

[173] Atar F B, Battal E, Aygun L E, Daglar B, Bayindir M and Okyay A K 2013 Plasmonically enhanced hot electron based photovoltaic device *Opt. Express* **21** 7196–201

[174] Knight M W, Wang Y, Urban A S, Sobhani A, Zheng B Y, Nordlander P and Halas N J 2013 Embedding plasmonic nanostructure diodes enhances hot electron emission *Nano Lett.* **13** 1687–92

[175] Li W, Coppens Z J, Besteiro L V, Wang W, Govorov A O and Valentine J 2015 Circularly polarized light detection with hot electrons in chiral plasmonic metamaterials *Nat. Commun.* **6** 8379

[176] Yang Y, da Costa R C, Fuchter M J and Campbell A J 2013 Circularly polarized light detection by a chiral organic semiconductor transistor *Nat. Photon.* **7** 634–8

[177] Zhang S, Zhou J, Park Y-S, Rho J, Singh R, Nam S, Azad A K, Chen H-T, Yin X and Taylor A J 2012 Photoinduced handedness switching in terahertz chiral metamolecules *Nat. Commun.* **3** 942

[178] Kenanakis G, Zhao R, Katsarakis N, Kafesaki M, Soukoulis C and Economou E 2014 Optically controllable THz chiral metamaterials *Opt. Express* **22** 12149–59

[179] Lv T, Zhu Z, Shi J, Guan C, Wang Z and Cui T 2014 Optically controlled background-free terahertz switching in chiral metamaterial *Opt. Lett.* **39** 3066–9

[180] Kanda N, Konishi K and Kuwata-Gonokami M 2014 All-photoinduced terahertz optical activity *Opt. Lett.* **39** 3274–7

[181] Zhu Y, Hu X, Chai Z, Yang H and Gong Q 2015 Active control of chirality in nonlinear metamaterials *Appl. Phys. Lett.* **106** 091109

[182] Kan T, Isozaki A, Kanda N, Nemoto N, Konishi K, Takahashi H, Kuwata-Gonokami M, Matsumoto K and Shimoyama I 2015 Enantiomeric switching of chiral metamaterial for terahertz polarization modulation employing vertically deformable MEMS spirals *Nat. Commun.* **6** 8422

[183] Wuttig M and Yamada N 2007 Phase-change materials for rewriteable data storage *Nat. Mater.* **6** 824–32

[184] Wełnic W, Pamungkas A, Detemple R, Steimer C, Blügel S and Wuttig M 2006 Unravelling the interplay of local structure and physical properties in phase-change materials *Nat. Mater.* **5** 56–62

[185] Wuttig M 2005 Phase-change materials: towards a universal memory? *Nat. Mater.* **4** 265–6

[186] Murata K, Aoki M, Suzuki T, Harada T, Kawabata H, Komori T, Ohseto F, Ueda K and Shinkai S 1994 Thermal and light control of the sol-gel phase transition in cholesterol-based organic gels. Novel helical aggregation modes as detected by circular dichroism and electron microscopic observation *J. Am. Chem. Soc.* **116** 6664–76

[187] Liu M, Hwang H Y, Tao H, Strikwerda A C, Fan K, Keiser G R, Sternbach A J, West K G, Kittiwatanakul S and Lu J 2012 Terahertz-field-induced insulator-to-metal transition in vanadium dioxide metamaterial *Nature* **487** 345–8

[188] Wang Q, Rogers E T, Gholipour B, Wang C-M, Yuan G, Teng J and Zheludev N I 2016 Optically reconfigurable metasurfaces and photonic devices based on phase change materials *Nat. Photon.* **10** 60–5

[189] Yin X, Schäferling M, Michel A-K U, Tittl A, Wuttig M, Taubner T and Giessen H 2015 Active chiral plasmonics *Nano Lett.* **15** 4255–60

[190] Li Z, Zhu Z, Liu W, Zhou Y, Han B, Gao Y and Tang Z 2012 Reversible plasmonic circular dichroism of Au nanorod and DNA assemblies *J. Am. Chem. Soc.* **134** 3322–5

[191] Schreiber R, Luong N, Fan Z, Kuzyk A, Nickels P C, Zhang T, Smith D M, Yurke B, Kuang W and Govorov A O 2013 Chiral plasmonic DNA nanostructures with switchable circular dichroism *Nat. Commun.* **4** 2948

[192] Kuzyk A, Schreiber R, Zhang H, Govorov A O, Liedl T and Liu N 2014 Reconfigurable 3D plasmonic metamolecules *Nat. Mater.* **13** 862–6